Deficits in Subprocesses of Visual Feature Search after Frontal, Parietal, and Temporal Brain Lesions—A Modeling Approach

Gisela Müller-Plath[1], Derek V. M. Ott[2], and Stefan Pollmann[3]

Abstract

■ Deficits in visuospatial attention are commonly observed after different kinds of brain lesions. However, the structure–function relationships are not well understood. We investigated whether our response time (RT) model, strategies of visual search (STRAVIS), combined with a linear model of brain lesions, enables us to relate specific impairments in cognitive processes to specific sites of focal brain lesions. In STRAVIS, RTs in overt visual feature search with graded target-distractor similarity are decomposed into the durations of successive search steps. Fitting the model to an observer's RTs yields individual estimates of the parameters "attentional focus size," "attentional dwell time," and "movement time of attention or the eyes." In 28 patients with various focal lesions to the frontal, parietal, and/or temporal cortex and 28 matched controls, we determined with the help of linear models which lesions were most predictive for each parameter. Predictions were validated with a second sample of 12 patients and 12 controls. Critical lesion areas for the STRAVIS focus size were the dorsolateral prefrontal cortex and the temporal lobe, with dorsolateral prefrontal cortex lesions reducing the focus and temporal lesions enlarging it. The STRAVIS dwell time was reduced in patients with lesions to the anterior insula and the superior parietal lobe. Lesions to the frontal eye fields, the superior parietal lobe, and the parieto-occipital cortex were most detrimental to the STRAVIS movement time. Applying linear models to a patient sample with heterogeneous lesions may be a promising new method for investigating how different brain areas interplay in a complex task. ■

INTRODUCTION

Patient studies have a long history in neuropsychology and are still an important tool to investigate structure–function relationships in the human brain. However, the diversity of individual lesions has been a constant problem in the interpretation of patient data. A typical approach to this problem is the analysis of overlapping lesion areas. Although this approach may yield important insights, especially when samples with mutually exclusive overlap areas are compared (e.g., Pollmann et al., 2007; Friedrich, Egly, Rafal, & Beck, 1998; Lamb, Robertson, & Knight, 1990), selection of the appropriate samples is often difficult, and the lesion variability outside the overlap regions is ignored (for details, see, e.g., Shallice, 1988).

Here, we present a mathematical modeling approach in which lesion variability is not regarded impedimental but instead used to gain insights into which brain areas might be crucial for a cognitive task and how they might interact. Two types of models are applied: On the side of the brain, presence or absence of lesions in different brain areas are linearly combined to predict cognitive measures. On the cognitive side, not only global behavioral measures are analyzed but the estimated parameters of a model that reflects cognitive subprocesses hypothetically underlying the behavior.

The topic of our analysis is visual search. Visual search is crucial for goal-directed orienting and acting in everyday life. It relies on selective attention in the feature as well as the spatial domain. Deficits in visual search are commonly observed in a variety of psychiatric and neurological conditions, for example, Parkinson's disease (e.g., Horowitz, Choi, Horvitz, Cote, & Mangels, 2006), schizophrenia (e.g., Davenport, Sponheim, & Stanwyck, 2006; Carr, Dewis, & Lewin, 1998), hemispatial neglect (e.g., Schindler, Clavagnier, Karnath, Derex, & Perenin, 2006; Sprenger, Kömpf, & Heide, 2002), autistic spectrum disorders (e.g., Greenaway & Plaisted, 2005), or Alzheimer's disease (for a review, Foster, 2001). In particular, one might expect such impairments after focal brain lesions to a network that is involved in carrying out visuospatial and selective attention tasks. In brain imaging studies, several frontal, parietal, occipital, and temporal regions have consistently been activated by such tasks, including the frontal and supplementary eye fields, the superior parietal lobule (SPL), intraparietal sulcus, TPJ, and the striate and extrastriate visual cortex (Corbetta, Patel, & Shulman, 2008; Müller-Plath, 2008; Corbetta & Shulman, 2002; Pollmann & von Cramon, 2000; Gitelman et al., 1999; Corbetta et al., 1998). Accordingly, visual search deficits have been demonstrated after lesions to various cortices (e.g., Mannan et al., 2005; Ptak

[1]Martin-Luther-University Halle-Wittenberg, [2]Max Planck Institute for Human Cognitive and Brain Sciences, [3]Otto-von-Guericke University Magdeburg

& Valenza, 2005; Humphreys & Riddoch, 2001; Husain et al., 2001; Greenlee, Berg, Stuhr, & Mergner, 2000; Eglin, Robertson, & Knight, 1991).

Mental activity in visual search is commonly viewed as interplay of several cognitive and perceptual subprocesses, like deploying attention to one or more items (i.e., attentional top–down modulation of perception within the so-called attentional focus), perceptually analyzing the items in the focus (including feature binding and/or comparing the input to a mental target template), shifting the attentional focus through space, decision making, and motor response. On the other hand, visual search tasks differ with respect to the number and the salience of target defining features, the number of targets and distractors in the display, and their spatial arrangement. The classical view, assuming a dichotomy between a parallel preattentive feature search and a serial attentive conjunction search (Treisman & Gelade, 1980), has been widely given up in favor of assuming a dynamical interplay and cooperation between parallel and focal mechanisms in all variants of search tasks (Chelazzi, 1999), with the above subprocesses being involved to different degrees. Accordingly, one might expect that a lesion to a distinct component of the abovementioned cortical network will affect specific cognitive subprocesses, so that, depending on the site and the extent of the lesion, the various search tasks are differentially affected. In contrast to studies comparing overall search behavior between different tasks, for example, feature and conjunction search (Nobre, Coull, Walsh, & Frith, 2003; Donner et al., 2002), the present study aims at diagnosing deficits in the subprocesses of a single task, namely, visual feature search.

Overt Visual Feature Search and the STRAVIS Model

In a typical visual search task, participants have to decide as fast as possible whether a predefined target is present in a set of distractor items or not. In feature search, the target is defined by a single perceptual feature (e.g., color or spatial frequency). If the target is sufficiently different from the distractors, usually a pop-out effect is observed; that is, the participant detects the target at first glance. When targets and distractors become more similar, the search becomes inefficient: The more similar the target to the distractor items, the steeper the slope of the RT becomes as a function of item number (e.g., Wolfe, 1994, 1998; Duncan & Humphreys, 1989; Treisman & Gormican, 1988).

In the RT slope, number and duration of search steps are confounded. In our earlier work, we developed and validated the RT model strategies of visual search (STRAVIS; Müller-Plath & Pollmann, 2003) that decomposes the RT in overt visual search tasks into the times of the hypothetically underlying successive subprocesses. Participants perform a feature search task with graded target-distractor similarity and various set sizes. Each experimental condition is represented by a model equation. Fitting the set of model equations to the set of empirical mean RTs of a participant yields individual parameter estimates for the average size of the attentional focus (number of items), the average dwell time of attention on each item group, the time for one movement of the attention and the eyes, and a time that is assumed constant across experimental conditions (e.g., initial display registration or motor response). STRAVIS has been developed and tested against alternative models with data from healthy subjects (Müller-Plath & Pollmann, 2003). It was successfully applied for analyzing fMRI data (Müller-Plath, 2008), and central model assumptions were validated with eye movement data (Heße, Wienrich, Melzer, & Müller-Plath, submitted).

Linear Modeling of Brain Lesions

In the present article, we applied an abbreviated version of the feature search task to patients who suffered from focal lesions to diverse frontal, parietal, and/or temporal cortex areas that, according to the literature, are involved in subprocesses of overt visual feature search and to a sample of matched controls. The participants' performance in these subprocesses was estimated with the help of STRAVIS. The relation between each subprocess and the brain lesions was formulated in a linear model (LM) with the lesion areas as (dichotomous) predictors and the respective STRAVIS model parameter as criterion. LMs were likewise fitted to the global behavioral measures *error rate* and *RT*, and the standard measure of visual search, the *RT slope*. For each criterion (three STRAVIS parameters plus error rate, RT, and RT slope), we then determined the subset of lesion areas that was best suitable for predicting the criterion. To avoid artifacts from stepwise methods of predictor selection, this was done with exhaustively comparing the LM fits between all possible subsets of predictors. For an independent validation of the resulting LMs, we recruited and tested a second sample of patients and controls. We compared their data collected in the task—the STRAVIS parameters as well as error rates, RTs, and RT slopes—to those that the LMs predicted from their brain lesions. Only for the three STRAVIS parameters but not for the global behavioral measures, LM predictions were validated. Thus, the LMs might indeed give a first coarse description on how the presence or the absence of various brain lesions affects subprocesses of visual feature search.

METHODS

Participants

Twenty-eight patients (7 women, 21 men) with visuospatial attention problems after a frontal, parietal, and/or temporal brain lesion and 28 age-matched controls (10 women, 18 men) participated in the original study. Visuospatial attention was assessed with the Test for Attentional Performance (Zimmermann & Fimm, 1994). A second sample

consisting of 12 patients (3 women, 9 men) and 12 controls (9 woman, 3 men) was tested for validating results. All patients were former or present outpatients of the Day Clinic for Cognitive Neurology, University of Leipzig, Germany. All participants gave written informed consent to the study. Included were patients with unifocal or multifocal lesions affecting at least one of the fronto-parieto-temporal cortex areas 1–7 as listed below. Excluded were patients with low-level vision deficits (visual acuity, contrast vision, or stereo vision), with visual field defects within 30° of visual angle, or with a field of gaze smaller than 90°. For this reason, occipital lobe lesions could not be investigated within the framework of the study. Patients with a visual hemineglect (clinical diagnosis and assessment with the Neglect Test; Fels & Geissner, 1996) and patients with memory or concentration problems impeding task execution, assessed with the d2 Test (Brickenkamp, 1962), the Trail Making Test (Reitan, 1958), and the Paced Auditory Serial Addition Test (Gronwall, 1977), were also excluded.

The age of the patients ranged from 23 to 73 years with a mean of 52.5 years, that of controls ranged from 24 to 69 years with a mean of 51.8 years. The second patient sample was aged between 38 and 62 years (mean = 51.9 years), and the second control sample aged between 23 and 61 years (mean = 49.0 years). The time interval between lesion event and testing ranged from 4 months to 22 years, with a median of 2.3 years. Clinical information was collected to establish the following variables: location(s) and lateralization of the lesion(s), etiology, and further brain pathologies, in particular subcortical lesions. The location(s) of the cortical lesion of each patient was coded in seven binary variables, representing seven areas of interest. In each, it was indicated whether the lesion affected the respective area (1) or not (0):

(1) dorsolateral prefrontal cortex (DLPFC): middle/superior frontal gyrus, BA 9/46 (n = 13);
(2) FEF: junction of superior precentral and middle frontal gyrus (Paus, 1996), BA 6 (n = 2);
(3) anterior insula, BA 13 (n = 17);
(4) inferior parietal lobule including the TPJ (IPL/TPJ): BA 22/40 (n = 11);
(5) temporal pole: BA 38 (n = 6);
(6) SPL: BA 7 (n = 4); and
(7) parieto-occipital: precuneus/cuneus, BA 7/19 (n = 3).

The individual data of the original sample are shown in Table 1. In relating them to the visual search performance, one has to keep in mind that lesions to the different areas do not occur independently of each other. Table 2 depicts the pairwise correlations of the seven lesion variables in the given sample and the results of the χ^2 tests of independence.[1] DLPFC lesions were significantly positively associated with lesions to the anterior insula and (marginally significantly) to the temporal pole and significantly negatively associated with parieto-occipital lesions. All other correlations failed significance ($p > .10$).

Stimuli, Task, Design, and Procedure

Stimuli were displayed on a 20-in. computer monitor with a viewing distance of 160 cm. Four, six, or eight items were presented equidistantly on an imaginary circle with 16 positions (see Figure 1A) and a diameter of 8° visual angle. All items were circular square-wave gratings with 1.3° visual angle diameter. Target items differed from distractor items in spatial frequency. The task was to decide as fast as possible whether there was a target present in the display or not and to press one of two response keys. Subjects were free to choose which two fingers they wished to use for responding. A factorial design with four factors was conducted. We varied the following:

(a) the task "search" versus "comparison." In the "search" task, the participant had to search for a target on any position in an arc of items that appeared on either the right of the left half of the screen. In the "comparison" task, the target could appear only on the top position of the screen, and the position of the arc was randomized around it. The participant had to decide whether the item on the top position was a target or not. (This condition was included for technical reasons to obtain a stable model fit; see Müller-Plath & Pollmann, 2003.)
(b) the similarity between target and distractors in spatial frequency in three levels (see Figure 1B);
(c) the set size in three levels: four, six, or eight items; and
(d) the target presence: two thirds of the trials contained targets.

The set size (c) was varied only in the task "search." In the "comparison" task, the set size was constantly six items. Apart from that, the design was full factorial.

Each trial began with a 1000-msec fixation cross, followed by the search display. The fixation cross appeared at the position of the upcoming (possible) target in the "comparison" task and in the center of the screen in the "search" task. During the search, participants were free to move their eyes. The display remained on the screen until the participant responded. The intertrial interval was 1000 msec. Trials were presented in blocks of constant task, similarity, and set size to allow the participant to adopt and to maintain an optimal search strategy for each condition. With three similarity levels and three "search" set sizes plus one "comparison" set size, 12 different blocks resulted. Within each block, target-present and target-absent trials were randomized. Wrongly answered trials were repeated once at the end of the block. Each block consisted of one dummy trial plus nine recorded trials plus the repeated trials. Three consecutive sessions were run, each comprising all 12 different blocks. Between blocks, breaks

Table 1. Patient Data: Gender, Age, Main Etiology of Lesion(s), Affected Brain Area(s), Lateralization, Distribution of Lesion, Size of Lesion, and Further Pathologies

No.	*Gender*	*Age*	*Etiology*	*(1) DLPFC*	*(2) FEF*	*(3) AntIns*	*(4) IPL/TPJ*	*(5) TPol*	*(6) SPL*	*(7) ParOc*	*LH*	*RH*	*Dist*[a]	*Size*[b]	*Further Pathologies*
102	m	53	Infarction	1	0	1	0	0	0	0	1	1	0	1	VLPFC
150	m	29	TBI	0	0	0	0	1	0	0	1	1	0	1	Fronto-polar
204	f	45	Infarction	1	0	0	1	0	1	0	1	0	1	1	
212	m	60	ICB	0	0	1	0	0	0	0	1	0	1	0	Left VLPFC
300	m	42	TBI	1	0	0	0	0	0	0	1	1	0	1	Fronto-polar, VLPFC
325	m	42	AVM	1	0	1	0	1	0	0	1	0	0	1	Bil. thal, left BG, VLPFC
342	m	34	TBI	1	0	1	0	1	0	0	1	1	0	1	Fronto-polar, bil. VLPFC
380	f	62	Infarction	0	0	1	1	0	0	0	0	1	0	0	
403	m	73	Infarction	1	0	1	0	0	0	0	1	0	0	0	Left VLPFC
432	f	23	AVM	0	0	0	0	0	0	1	1	0	0	0	Left thal, CC
441	m	60	Infarction	0	0	0	1	0	1	0	1	0	0	1	
446	m	62	Infarction	1	0	0	0	0	0	0	1	0	0	0	Left VLPFC
550	m	71	Infarction	1	0	1	0	0	0	0	1	0	0	1	Left VLPFC
583	m	66	Infarction	0	0	0	0	0	1	1	1	0	0	0	Left frontal WM
662	m	61	Infarction	0	0	0	1	0	0	0	1	0	1	1	
718	m	59	ICB	0	0	1	0	0	0	1	1	0	0	1	
721	m	63	Subdur hem	0	1	0	0	0	0	0	0	1	0	1	Fronto-polar
739	m	38	Infarction	0	0	1	1	0	1	0	1	0	0	1	
749	f	56	Infarction	0	0	1	0	0	0	0	1	0	0	0	
753	m	53	Infarction	0	0	1	0	1	0	0	0	1	0	0	Right VLPFC
760	m	41	Infarction	1	0	1	1	1	0	0	1	0	1	0	Left VLPFC
790	f	57	Infarction	1	0	1	1	0	0	0	0	1	0	0	Right BG, thal
854	f	50	Infarction	1	0	1	0	0	0	0	0	1	0	1	right BG, thal, VLPFC
1115	m	65	Infarction	0	0	1	1	0	0	0	0	1	0	1	
1224	m	27	Infarction	1	0	1	1	1	0	0	0	1	1	0	Right VLPFC, arachnoid cyst
1561	m	67	Infarction	1	1	1	0	0	0	0	1	0	0	1	Left VLPFC
1597	m	57	Infarction	0	0	0	1	0	0	0	1	0	0	0	Right thal, BG
1607	f	54	Infarction	0	0	0	1	0	0	0	1	0	0	0	
n				13	2	17	11	6	4	3	21	11	5	15	

AntIns = anterior insula; TPol = temporal pole; ParOc = parieto-occipital; TBI = traumatic brain injury; ICB = intracerebral bleeding; AVM = arteriovenous malformation; LH = left hemisphere; RH = right hemisphere; bil. = bilateral; WM = white matter; BG = basal ganglia; thal = thalamic nuclei; VLPFC = ventrolateral prefrontal cortex (inferior frontal gyrus).

[a]Distribution of lesion: 0 = unifocal, 1 = multifocal.

[b]Size: 0 = small, 1 = large according to expert rating.

Table 2. Pairwise Correlations between (Binary) Lesion Variables and Significance of Association

	DLPFC	*FEF*	*Ins*	*IPL/TPJ*	*TPol*	*SPL*	*ParOc*
DLPFC	1	−.02	.42*	−.28	.31*	−.23	−.37**
FEF		1	−.06	−.22	−.14	−.11	−.10
Ins			1	−.10	.24	−.30	−.19
IPL/TPJ				1	−.06	.30	−.28
TPol					1	−.21	−.18
SPL						1	.19
ParOc							1

Note that for two binary variables, $r^2 = \phi^2 = \chi^2 / n$.

Ins = insula; TPol = temporal pole; ParOc = parieto-occipital.

p value of χ^2 test ($df = 1$): *$p < .10$; **$p < .05$; ***$p < .01$; ****$p < .001$.

were allowed. The first session was a training session containing a demonstration display at the beginning of each block, in which the task was explained and the target shown. Blocks were ordered in increasing difficulty, starting with the easiest condition (Comparison, Similarity Level 1, Set Size 4) and ending with the most difficult condition (Search, Similarity Level 3, Set Size 8). The two recorded sessions were identical, except that in the last session the block order was reversed. Depending on individual RTs, errors, and lengths of breaks, the total testing time was between 40 and 60 min. In each of the 12 experimental conditions, 18 regular trials were recorded, 12 of which contained a target.

For the most dissimilar target, we expected a pop-out search, reflected in a flat RT curve across set sizes. For targets more similar to the distractor, we expected the search to become increasingly inefficient, which should be reflected in an increasing slope of the RT function.

Behavioral Data Analysis

Error rates in the visual search task were computed individually across the regular trials of each block (repetition trials not included). For RT analysis, we included only trials in which a target was present and correctly identified (12 trials per experimental condition minus the number of trials wrongly answered twice). For each participant and each condition, outlier RTs outside ±2 *SD*s from the mean were excluded if existing (in most cases, there were none), and the remaining RTs were averaged. Each participant thus delivered a set of 12 error rates and a set of 12 RT means as measures of his or her observed overall performance in the task (3 × 3 "search" + 3 "comparison" conditions). The RT slopes were obtained from linear regressions of the "search" RTs onto the set size at each of the three similarity levels.

Describing Visual Search Processes: The STRAVIS Model

A set of 12 model equations was fitted to the 12 RT means of each participant. Because the STRAVIS model has been extensively described in a previous article (Müller-Plath & Pollmann, 2003), we give only a brief overview here. STRAVIS is a two-stage model, in which the stationary deployments of attention and spatial attentional shifts (in overt search, usually accompanied by eye movements) alternate. Integrating elements from Guided Search 2.0 (Wolfe, 1994) and the Attentional Engagement Theory (Duncan & Humphreys, 1989, 1992), the central assumption of STRAVIS is an attentional focus of variable size. Further, an attentional dwell time of variable duration is assumed. The attentional focus denotes the subset of items to which attention is deployed in parallel to decide whether to terminate the search or to move on. The maximum size of the focus, which a subject can search the display accurately with, results from a "saliency map" (synonym "activation map") computed in parallel across the whole display.[2] It depends not only on physical values like the target-distractor similarity and on the number of homogeneous distractors but also on perceptual and attentional capacities of the subject. With increasing target-distractor similarity and with decreasing number of homogeneous distractors, the maximum focus size decreases (see Figure 2, upper panel).[3] Moreover, we assume that

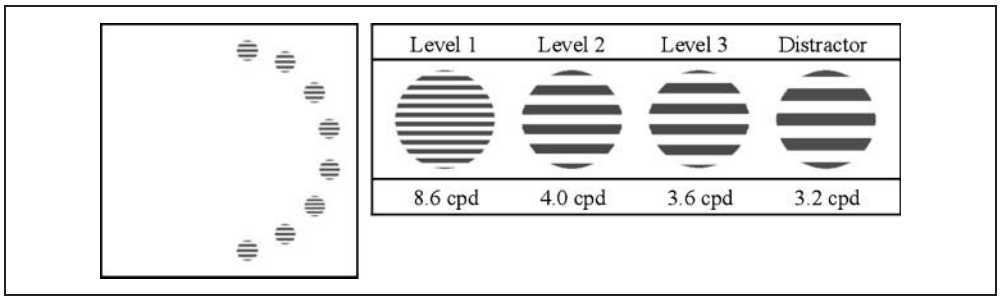

Figure 1. (A, left panel) Example of a search display. In the comparison task, where the target was always at the top position, the position of the arc of distractors was randomized. (B, right panel) Appearance and physical values of the target item in the three similarity levels and the (homogeneous) distractor items. In all items, the width of the first horizontal stripe was randomized so that subjects could not use it for item discrimination.

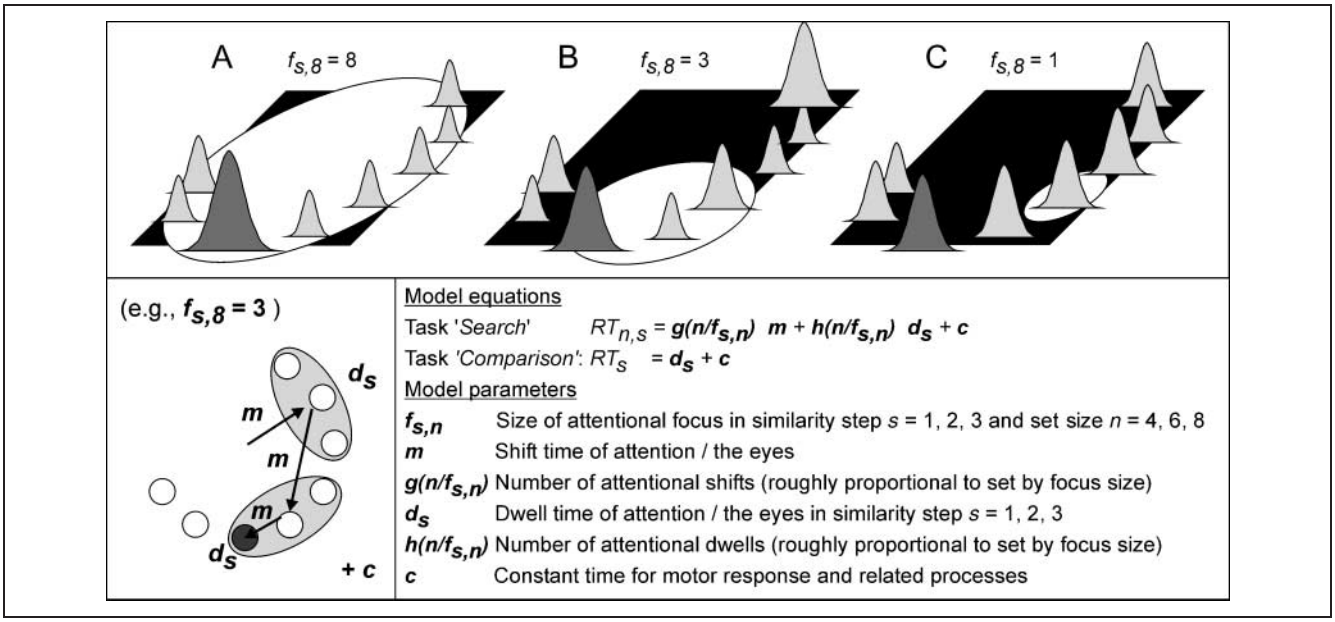

Figure 2. Upper panel: Concept of a saliency map and an according size of the attentional focus. Lower panel: Hypothetical search process and model parameters according to STRAVIS. For details, especially on the functions g and h specifying the mean number of movements and dwells in a trial as a function of the focus size and set size, see Müller-Plath and Pollmann (2003).

the focus size is open to conscious control: If the subject knows in advance how target and distractors will look like, he or she can adjust the focus to an adequate size. The optimal focus size depends thus on intact "preattentive" perceptual feature processing as well as on intact attentional control processes.

In the model, the RT in each trial is decomposed into the times of subprocesses that are assumed to interact in quick alternation during task execution. The "search" task is assumed to consist of the subprocesses *onset registration*, *selection*, *shift*, and *response*: After the initial *onset registration*—and simultaneously or subsequently (see Footnote 2) to the computation of a saliency map—attention selectively modulates perceptual sensitivity to the relevant feature and assesses this feature within a "focus of attention" (subprocess selection). If the target feature is not detected within the focus, a movement of spatial attention is prepared and executed based on the saliency map, usually accompanied by a saccade (subprocess shift). When the target is found or when the participant decides that there is none, a motor *response* is prepared and executed. Selection and shift take place the more often the smaller the attentional focus is. The "comparison" task, which was included mainly for technical reasons (see above), is supposed to comprise only the subprocesses *onset registration*, *selection*, and *response*, each occurring once and the selection being of constant spatial size.

The supposed cognitive subprocesses are conceptualized in the model parameters as follows: In the subprocess *selection*, attention modulates perception within the attentional focus for a certain time duration, the dwell time. During the dwell time, all items within the focus are compared with each other (and to a target template) in parallel, and a decision is prepared whether to move on with the search. Because we assume a large overlap of attentional modulation, perceptual comparison, and decision, these processes are all subsumed under the term selection. The size of the attentional focus is assumed to vary stochastically, with its mean $f_{s,n}$ depending on the target-distractor similarity s (s = 1, 2, 3; see Figure 1B) and the set size n. The value $f_{s,n}$ indicates how many items are on average selected in parallel. In case of pop-out search, $f_{s,n}$ equals the set size; that is, all items in the display are selected in one step. At the other pole of the continuum, $f_{s,n} = 1$ denotes strictly serial search; that is, the items are selected one by one. The attentional dwell time d_s (s = 1, 2, 3) is assumed to depend on the target-distractor similarity.

For the subprocess *shift*, a constant time amount m is assumed, independent of how far attention (and the eyes) are moved. Although saccade durations are linearly related to saccade lengths, this relation is negligible in the spatial range covered by the display (for details, see Müller-Plath & Pollmann, 2003).

The total RT in an experimental trial is modeled as the sum of the attentional/eye movement time (duration m) multiplied by the number of movements, the dwell time on each group of items (duration d_s) multiplied by the number of dwells, and a constant time c that comprises all processes that occur only once in a trial and are independent of the experimental condition. The lower panel of Figure 2 shows a simplified form of the RT equations for the tasks "search" and "comparison" and gives a list of the model parameters.[4] For each participant, the set of STRAVIS model equations were fitted to the 12 RT means

with a weighted least squares algorithm (Müller-Plath & Pollmann, 2003; see also Figure 2), yielding individual parameter estimates for $f_{s,n}$, d_s, m, c. The estimated focus sizes $f_{s,n}$ and the estimated dwell times d_s were averaged across the similarity levels $s = 1, 2, 3$ (and the set sizes $n = 4, 6, 8$). Each participant was thus finally assigned four parameter values as measures of the efficiency of the hypothetical subprocesses *selection* (capacity: focus size f; time duration: dwell time d), *shift* (movement time m), and *onset registration/response* (constant time c).

Looking at the equations in Figure 2, one might suspect that the correct estimation of the focus size crucially depends on the assumption that the dwell and the constant times (parameter d_s and c) agree between the search and the comparison task. However, this is not the case because the focus size was modeled as depending on the similarity and the set size, whereas the dwell time depended on similarity only. Empirically, we compared tasks with and without the comparison condition in our earlier work (Müller-Plath, 2000; Experiments 1 and 2). Without the comparison condition, it was not possible to reliably separate the movement time from the constant time and from the dwell time in Similarity Level 1. However, the differences between the dwell times and the focus size estimations were preserved. Second, we validated the focus size estimations with an independent experiment (Müller-Plath & Pollmann, 2003, Experiment 2), in which a subset of item positions was cued before the items appeared. For every subject, search times were flat for subsets smaller or equal the estimated focus size and rose as soon as the cue size exceeded the estimated focus size. In a recent eye movement study (unpublished), we were further able to roughly confirm the assumption of identical dwell and constant times between the two types of tasks.

Let us remark here that abnormal parameter values can be interpreted according to the model assumptions: A reduced focus size might result from perceptual feature processing being ineffective, so that saliency maps are less informative, or from attentional control processes being impaired, so that anticipative top–down adjustment of the focus size is hampered. The latter might as well result in an inadequately large focus. The dwell time will be prolonged if attentional modulation of perception is ineffective, if perceptual comparison of features is impaired, or if decision making is slowed. A prolonged movement time may indicate difficulties in disengaging attention, possibly resulting from computation of spatial coordinates for the movement ("where") being ineffective or from saccade initiation being disturbed ("when"; see Findlay & Walker, 1999). The constant time will be prolonged if the start of searching behavior is delayed or if response execution is slowed.

Analyzing Brain Lesion Effects: Linear Models

Visual search data were evaluated at two levels: the level of observed performance and the STRAVIS model level. The observed performance was assessed by means of error rates, RTs, and RT slopes. At the model level, the individually estimated parameter values of STRAVIS were analyzed (focus size, dwell time, and movement time), which are supposed to reflect measures of performance in the hypothetical attentional subprocesses of visual search (see Figure 2). Thus, altogether, six dependent measures (DMs) were assessed. Three different types of analyses were run on them:

(1) We compared the DMs between patients and controls to check whether the lesions had any effect at all.
(2) Because the lesions did not occur independently of each other (Table 2), we did not run separate significance tests on these effects. Instead, to investigate which brain lesions might be most predictive for the observed deviations from normality and how their specific effects might be quantified, we formulated an LM for each DM in which the seven brain area variables served as predictors. For each DM Y, let the full LM be, $\boldsymbol{Y} = \beta_0 + \sum_{j=1}^{7} \beta_j \boldsymbol{X_j} + \boldsymbol{\varepsilon}$, where $\boldsymbol{X_1}, \ldots, \boldsymbol{X_1}$ denote the binary lesion variables 1–7, and $\boldsymbol{\varepsilon}$ is the vector of individual errors (see Appendix A). For each DM, a subset of predictors was then selected that explained a maximum amount of variance with a minimum number of predictors. This was achieved by the following procedure (which circumvents most sources of artifacts of stepwise methods; see for example, Hocking, 1996): First, we fitted all possible subsets of predictors. For each subset size (i.e., for one to seven predictors), we then selected the subset that maximized R^2. To decide between the so-selected seven models, we tested first whether each model accounted for a significant portion of variance. Second, we tested each model against its immediate submodel. Finally, we applied several criteria suggested in the literature that relate the portion of variance accounted for to the number of predictors: Mallows' Cp (Mallows, 1973), Akaike's information criterion (Akaike, 1974), and adjusted R^2. In case the three criteria agreed on the same subset of predictors, we chose this as the most conclusive LM provided it explained a significant ($\alpha = .05$) portion of variance. Otherwise, we kept a priori the sparser one of the suggested models unless a larger one explained significantly more variance ($\alpha = .05$). Although this procedure ensures optimal model selection in the given sample, it is still prone to sampling error, in particular when the initial number of predictors is large compared with the number of cases and when predictors are intercorrelated. Therefore, we kept the second-best model for the chosen number of predictors in the analysis as well.
(3) For the same reason, we subjected the LMs to further statistical tests. First, two "within-sample validations" were performed:

    (I.i) The observed mean DM of those patients that were declared unimpaired by the model (M_0) was compared with that of the control subgroup (M_c).

(I.ii) The residual variance in the subgroup of patients ($\hat{S}^2_{Res,p}$) was compared with the observed variance in the subgroup of controls ($\hat{S}^2_c$). The underlying idea was that each DM shows considerable variation in the normal population. One can thus not expect that variance in patients is completely explained by their brain lesions. Instead, we regarded a model appropriate that explained so much variance that the residual variance in patients equaled the variance in controls.

Both comparisons were expected to reveal no difference. We computed 90% confidence intervals (I.i) for the difference of the expected subsample means $E(M_0) - E(M_c)$, which should contain 0 if the model were true, and (I.ii) for the ratio of the expected residual (unexplained) variance in patients and the expected variance in controls $\frac{E(\hat{S}^2_{Res,p})}{E(\hat{S}^2_c)}$, which should contain 1 if the model were true. For details on the construction of the two types of confidence intervals, see the Appendix A.[5]

Second, we conducted a cross validation by applying the models to a new sample of patients and controls. The underlying idea was that if an LM held, it should reliably predict mean and variance of patients with any combination of brain lesions that served as predictors in the model. The rationale of the tests presented in this section requires a little more formalism (for an illustration, you may consult Figure 5 in the Results section). In an LM with m binary predictors, the 2^m different predictor combinations (the combinations of lesions) define so-called "prediction levels" (vertical lines in Figure 5). For subjects at level k, the equation $\hat{y}_{(k)} = \hat{\beta}_0 + \sum_{j=1}^{m} \hat{\beta}_j \cdot x_{(k),j}$ describes the proposed linear association between the predicted mean DM and the presence of lesions in the m brain areas selected as relevant. For cross validation, we computed the so-called "prediction intervals" for the data of new samples:

(II.i) the interval around $\hat{\beta}_0$ that should contain the sample mean M_{c2} of a new control sample with probability .90 if the model were true; and

(II.ii) the intervals around the predicted values $\hat{y}_{(k)}$ that should contain the DM of a new patient at predictor level $k \in \{1,\ldots, 2^m\}$, that is, with a given combination of lesions, with probability .90 if the model were true. This was done for all possible lesion combinations. Because for any new patient, probability is .90 that his or her value would be within the respective interval, in total about 90% of the new data (i.e., about 11 of the 12 patients) should be comprised by these intervals and mispredictions can be systematically analyzed. However, to account for all new patients simultaneously, we also computed the Bonferroni-adjusted prediction intervals (which were larger by a certain factor). Here, the global probability that *all* observations are within their respective interval is .90 if the model is true. Model validation was regarded failed if there was any new observation falling outside its .90 Bonferroni-adjusted prediction interval. Details on the computation of the intervals are provided in the Appendix A.

Because we were interested in telling apart the effects of the lesions onto the distinct subprocesses of attention, the six DMs were assessed independently of each other. All statistical computations were run with the software R (R Development Core Team, 2008).

RESULTS

The numbering in this section refers to the numbering in the last part of the Methods section.

Performance of Patients and Controls

Observed Performance

Figure 3A depicts the error rates and the RTs of patients and controls in the 12 experimental conditions. For both measures, we conducted separate 2 × 3 × 3 ANOVAs with the between-subjects factor Group (patients/controls) and the within-subjects-factors Similarity (target-distractor similarity levels 1, 2, and 3) and Set Size (search set sizes 4, 6, and 8) with the Huyn–Feldt corrections of degrees of freedom. The data of the "comparison" condition were not included in this analysis.

The error rate increased significantly with the similarity and the set size. The steeper the increase with the set size, the more similar the target was to the distractors: main effect of Similarity, $F(1.8, 100) = 44.8, p < .001$; main effect of Set Size, $F(2,108) = 5.54, p = .012$; Similarity × Set Size interaction, $F(3.3, 177) = 2.49, p = .044$. Patients made on average more errors than controls, but the difference failed significance: main effect of Group, $F(1,54) = 2.51$, $p = .119$. The increase of errors with increasing similarity and with increasing set size was not significantly stronger in patients than in controls: Group × Similarity interaction, $F(1.9, 100) = 2.10, p = .132$; Group × Set Size interaction, $F(2,108) = 2.22, p = .166$. The Group × Similarity × Set Size interaction failed significance, $F(3.3, 177) = .38, p = .826$.

The RT also increased significantly with the similarity and the set size, and again the steeper the increase with the set size, the more similar the target was to the distractors: main effect of Similarity, $F(1.4, 75.9) = 162, p < .001$; main effect of Set Size, $F(2,108) = 95.6, p < .001$; Similarity × Set Size interaction, $F(2.7, 145) = 31.3, p < .001$. The mean RT in patients was significantly longer than in controls: main effect of Group, $F(1,54) = 7.2$, $p = .010$. The increase with the similarity and also with the set size was marginally significantly stronger in patients than in controls: Group × Similarity interaction, $F(1.4, 75.9) = 3.05, p = .071$; Group × Set Size interaction,

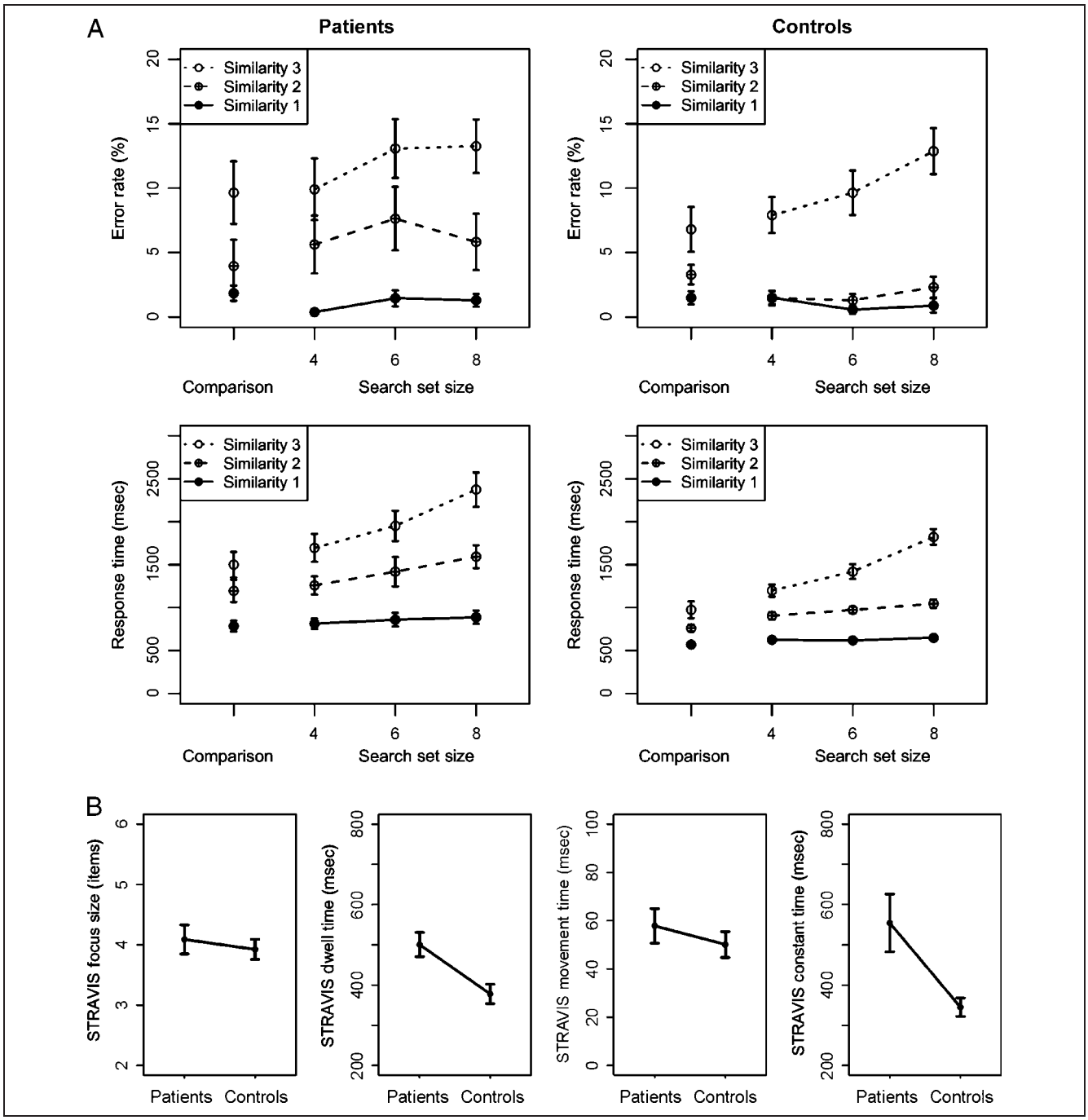

Figure 3. (A) Error rates and RTs, and (B) STRAVIS parameters in patients and controls. Error bars give the *SEM*s.

$F(2,108) = 2.59, p = .080$. The three-way Group × Similarity × Set Size interaction was not significant, $F(2.7, 145) = .77, p = .50$.

In both groups, the error rate as well as the RT reflected the increase in search difficulty with increasing target-distractor similarity and with increasing set size.

STRAVIS Model Parameters

After having established that the patients performed the visual search task only marginally less accurately but more slowly and less efficiently than controls, the nature of the latter differences was explored by analyzing the STRAVIS model parameters. First, we assessed the model fit errors to make sure that participants searched the array in a systematic fashion as proposed by STRAVIS. In patients, STRAVIS explained on average 91.6% (range = 78–98%) of the variance of the 12 individual RT means compared with 93.8% (range = 78–99%) in controls. In both groups, we regarded the model fit satisfactory for interpreting the parameters.

The STRAVIS parameter values for focus size, dwell time, movement time, and constant time are supposed to reflect the individual efficiency of the hypothetical attentional

subprocesses *selection* (capacity and speed), *shift* (speed), and *initial perception/response* (speed; see previous section). Figure 3B contrasts the values of patients and controls. According to the STRAVIS focus sizes, dwell times, and movement times, the hypothetical performance of visual-attentional processes in total differed significantly between patients and controls [$F(3,52) = 3.18$, $p = .032$, two-group MANOVA with three dependent variables]. Thus, the above-observed differences in RT and RT slope seem not only due to nonattentional processes [which are hypothetically covered by the STRAVIS constant time, which was also prolonged in patients; $t(54) = 2.72$, $p = .009$]. When looking at intercorrelations between the STRAVIS parameter values, we found the correlation between focus size and movement time to be $r = .20$ in patients and $r = .47$ in controls. The positive correlation might indicate that persons scanning the display with a larger focus make on average fewer and larger movements, which take more time. The correlation between focus size and dwell time was $r = .23$ (patients) and $r = .04$ (controls) and between dwell time and movement time was $r = .43$ (patients) and $r = -.24$ (controls). Dwell and movement time being positively correlated is counterintuitive, given the STRAVIS model assumptions. In patients, lesions that prolong the dwell time and those prolonging the movement might either be identical or co-occur in a large part of the sample.

Establishing Possible Associations between Subprocesses of the Search and Brain Lesions

In the preceding paragraph, we found patients with various fronto-parieto-temporal lesions showing an inferior level of performance in observed as well as hypothetical measures of visual feature search compared with controls. The following analysis aims at the question how the brain areas under investigation might interplay in carrying out the cognitive subprocesses underlying these measures. The six DMs of this study—the two observed measures error rate and RT, the standard efficiency measure RT slope, and the three individually estimated STRAVIS parameters focus size, dwell time, and movement time—were evaluated separately. For each of the six DMs and the seven brain areas under investigation, a pair of plots in Figure 4 contrast the mean DM of patients with a lesion in the given area to that of patients without and show both in relation to the control group mean. To shed light on the question of which lesion areas were most predictive for the observed differences between patients and controls in each of the DMs and how their effects might be quantified, we used the seven binary lesion variables as predictors in LMs that were fitted to the DMs.

The full set of seven predictors was then reduced so that a maximum portion of variance was accounted for with a minimum number of predictors. For all DMs (with a single exception for the error rate, see Table 3), the sequence of selected models with one to seven predictors was ordered in the sense that every model in the sequence was a supermodel to its predecessor, which is not a trivial result when using the exhaustive—and not a stepwise—method of predictor selection. It is further noteworthy that the coefficient estimates were quite stable across differently large models. Third, for three of the six DMs (the three STRAVIS model parameters), the three selection criteria, although based on very different theoretical grounds, agreed on the same subset of predictors. Finally, when F tests were performed to compare each model against its immediately preceding submodel (if existing among the selected models), for all models bigger than the favored ones, F dropped sharply, mostly to values below 1. These patterns might all be interpreted as indications of the suggested solutions being quite robust. Table 3 shows for each DM the selected LM, the second-best model with the same number of predictors, the R^2, the significance levels of R^2 being larger than zero, of the linear coefficients being different from zero, and which of the predictor selection criteria (Akaike's information criterion, Mallow's Cp, and adjusted R^2) favored the model.

The left-hand panel of Figure 5 graphs the sample data of patients and controls together with the hypothesized distributions of the DMs according to the favored LMs (predictor selections and coefficient estimates). They illustrate the proposed linear associations as follows: Below the graph, the 2^m predictor levels are shown. The theoretical means $\mu_{(k)}$ in the respective subpopulations are indicated by the line with slope 1 through the origin. The horizontal position of each depicted subsample shows the estimation of $\mu_{(k)}$ by $\hat{y}_{(k)}$, that is, the LM prediction, and the average vertical position of the data points shows the estimation of $\mu_{(k)}$ by the subsample mean $M_{(k)}$ (see Methods section). If there were associations other than linear, the subsample means should exhibit systematic deviations from this line. The portion of variance R^2 explained by an LM can be visualized in the diagram if one compares the residual (i.e., unexplained) variance in the subsamples to the variance in the patient sample as a total. One might further judge from the diagram whether the equal variance assumption across subpopulations seems plausible. Because the sample sizes in the subgroups of patients were occasionally very small, we refrained from testing these notions statistically.

For the error rate, the seven brain lesion variables accounted altogether for .27 of the variance. One single predictor explained already .21 of it: a lesion to the temporal pole. According to this model, the percentage of errors, which was estimated on average 5.1% in controls, was estimated to rise by on average 9.3 percentage points in case of a temporopolar lesion. All other predictors were negligible in this context. The second-best model, which predicted the error rate from insular lesions, accounted only for .06 of the variance. (Here one might think about adding more predictors; however, then temporal

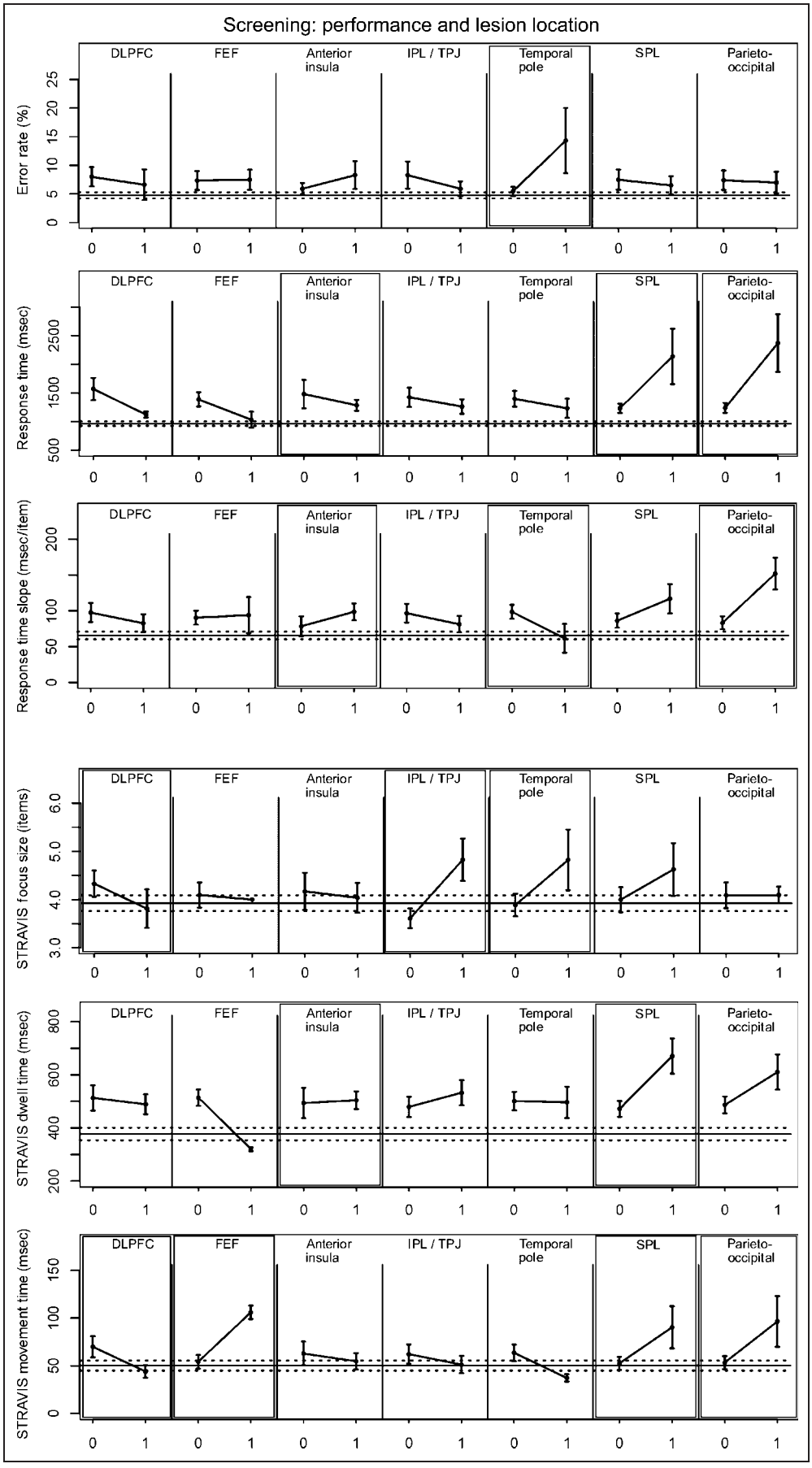

Figure 4. Impact of lesions on the seven areas under investigation: For each of the six DMs, the mean DM of patients with a lesion in the given area is shown in contrast to that of patients without. The *SEM* in the patient subgroups is indicated by error bars, in the control subgroup by continuous lines. Areas selected as relevant predictors in the linear modeling (see next section) are framed.

Table 3. Linear Modeling of the Six DMs with the Seven Binary Lesion Variables as Predictors

							Validation			
							Within-sample		*New Sample*	
							90% Confidence Interval		*Content of the .90 Prediction Interval*	
Model					*Assessment*		*(I.i) Difference of Means between "Unimpaired" Patients and Controls*	*(I.ii) Ratio of Residual Patient Variance and Control Variance*	*(II.i) The Sample Mean of the n = 12 Controls*	*(II.ii) x of the n = 12 Patient Values (All Patient Values Are within the Bonferroni-adjusted Interval)*
$\hat{\beta}_0$	$\hat{\beta}_1$	$\hat{\beta}_2$	$\hat{\beta}_3$	$\hat{\beta}_4$	R^2	*Favored by*				
Error Rate (%)										
5.1****	**TPol 9.3******				**.21******	**Cp, AIC**	**(−0.9, 2.3)**	**(3.48, 12.8)[a]**	**No[a]**	***x* = 10 (yes)**
5.1****	AntIns 3.2*				.06*		(−0.7, 3.0)	(4.28, 15.7)[a]	No[a]	*x* = 11 (yes)
RT (*msec*)										
991****	**AntIns 182***	**SPL 842******	**ParOc 1039******		**.54******	**Cp, AIC**	**(−136, 158)**	**(2.44, 9.21)[a]**	**Yes**	***x* = 7 (no)[a]**
1022****	TPol 210	SPL 850****	ParOc 1067****		.53****		(53, 349)[a]	(2.48, 9.36)[a]	Yes	*x* = 6 (no)[a]
RT Slope (*msec per item*)										
67****	**AntIns 39*****	**TPol −37****	**ParOc 73*****		**.34******	**Cp**	**(−15, 25)**	**(1.08, 4.10)[a]**	**Yes**	***x* = 8 (no)[a]**
64****	AntIns 29***	SPL 29	ParOc 69***		.30****		(−29, 15)	(1.19, 4.32)[a]	Yes	*x* = 10 (no)[a]

STRAVIS Focus Size (*Items*)										
3.8****	**DLPFC −0.7****	**IPL/TPJ 1.0*****	**TPol 1.1****		**.24*****	**Cp, AIC, R_{adj}^2**	**(−0.6, 0.7)**	**(.79, 2.98)**	**Yes**	***x* = 12 (yes)**
3.8****	AntIns −0.5	IPL/TPJ 1.1***	TPol 1.0**		.22***		(−1.2, 0.2)	(.84, 3.17)	Yes	*x* = 10 (yes)
STRAVIS Dwell Time (*msec*)										
391****	**AntIns 98****	**SPL 255******			**.25******	**Cp, AIC, R_{adj}^2**	**(−55, 122)**	**(.72, 2.67)**	**Yes**	***x* = 12 (yes)**
411****	TPol 85	SPL 259***			.20***		(−17, −155)[a]	(.78, 2.90)	Yes	*x* = 11 (no)[a]
STRAVIS Movement Time (*msec*)										
51****	**DLPFC −14**	**FEF 62*****	**SPL 35*****	**ParOc 34***	**.28*****	**Cp, AIC, R_{adj}^2**	**(−16, 25)**	**(.63, 2.41)**	**Yes**	***x* = 11 (yes)**
49****	TPol −12	FEF 57**	SPL 32*	ParOc 37*	.26***		(−18, 16)	(.77, 2.18)	Yes	*x* = 10 (yes)

For each DM, the predictor selection and coefficient estimates of the best model (boldface) and the second-best model with same number of predictors (plain face) are shown together with their significance level. The "Assessment" columns give the proportion of variance accounted for by the model and by which of the three applied regression criteria the model was favored. The "Validation" columns show the results of model validation within the sample and in a new sample of patients and controls. The confidence intervals (I.i-ii) were supposed to contain the 0 and 1, respectively, if the model held (for details, see text).

Cp = Mallows' Cp; AIC = Akaike's information criterion; R_{adj}^2 = adjusted R^2; AntIns = anterior insula; TPol = temporal pole; ParOc = parieto-occipital.

[a]Result deviating from expectation.

*$p < .10$

**$p < .05$.

***$p < .01$.

****$p < .001$.

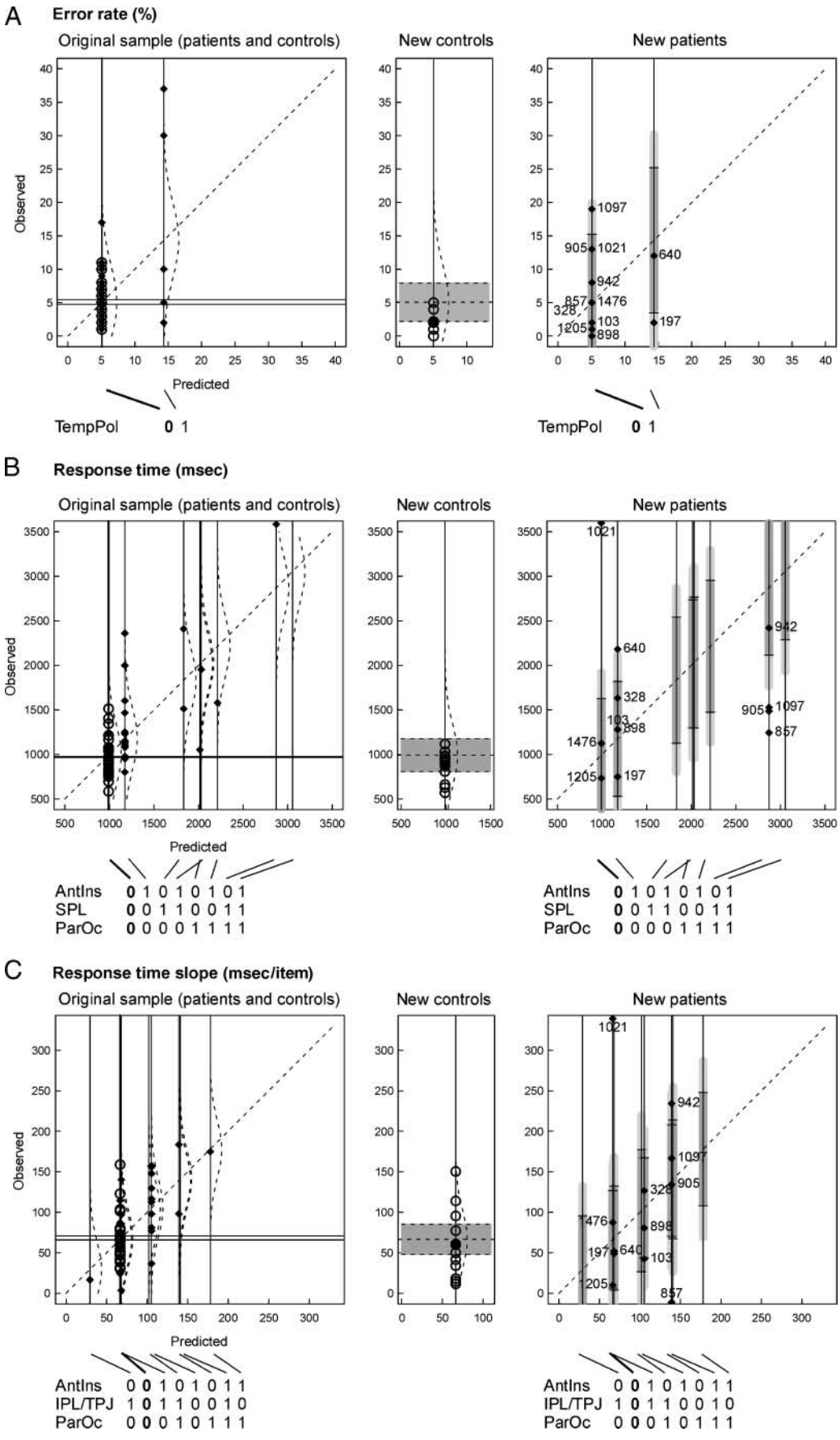

pole came in again, and we arrived at the model already selected as best.)

Regarding the RT, the seven predictors accounted altogether for .56 of the variance. Remarkably, from one to seven predictors, all selected models were highly significant ($p < .001$), but three predictors (anterior insular, SPL, and parieto-occipital lesions) sufficed to explain this variance almost entirely. According to this model, the mean RT, which was estimated 991 msec without lesions, should rise by 182, 842, and 1039 msec with insular, SPL, and parieto-occipital lesions, respectively.

Regarding the RT slope, the seven predictors altogether explained .37 of the variance. Here, the three selected predictors were the anterior insula, the temporal pole, and the parieto-occipital cortex. The mean RT slope was estimated 67 msec per item without any of these lesions and was predicted to rise by 39 and 73 msec per item with anterior insular and parieto-occipital lesions, respectively, and to drop by 37 msec per item with a lesion to the temporal pole.

Because the portion of RT variance accounted for by the lesions was quite large, it was of particular interest whether the STRAVIS parameters could provide information in more detail which lesion might have affected which of the subprocesses hypothetically contributing to the RT and RT slope.

The STRAVIS focus size was best predicted by three lesion areas, accounting for $R^2 = .24$ of the variance (all seven lesion areas together accounting for .26). The mean focus size in the absence of any lesions was estimated 3.8 items. According to the LM, lesions to the DLPFC should reduce the mean focus size by .7 items, whereas lesions to the temporal lobe (IPL/TPJ area and temporal pole) should enlarge it by 1.0 and 1.1 items, respectively. Because in most of our patients the DLPFC lesion extended into the ventrolateral part of the prefrontal cortex (VLPFC, see Table 1), it was difficult to distinguish the impact of either. However, two patients had only the VLPFC lesioned, and results were weakened when we coded any LPFC lesion with 1. We thus suggest that the dorsolateral portion of PFC being lesioned is crucial.

For the STRAVIS dwell time, the zero lesion estimate was 391 msec. The seven lesion areas together accounted for .32 of the variance. A two-predictor model was favored, explaining .25 of the variance. It suggested an average increase of the dwell time by 98 msec with lesions to the anterior insula and by 255 msec with lesions to the SPL.

For the STRAVIS movement time, a mean value of 51 msec was estimated for persons without lesions. All seven lesion areas together accounted for .31 of the variance. The favored model contained DLPFC, FEF, SPL, and parieto-occipital lesions as predictors, altering the mean movement time by −14, +62, −35, and +34 msec, respectively, and accounting for .28 of the variance.

It should be noted that the above coefficient estimates were not based on the partly very small subsamples (e.g., $n = 2$ patients with FEF lesions) but reflect the geometrical structure of the entire 56 data points projected onto a one- to four-dimensional predictor space. However, estimates might be influenced by outliers. To strengthen empirical evidence, we subjected the LMs (coefficient selection and estimation) to further tests.

Model Validation

To further validate the LMs proposed above, we recruited and tested a new sample of 12 patients and controls each. For details on the patients, see Table 4. We used the LMs obtained above for predicting visual feature search performance of the new subjects, again at two levels of data: the level of observed performance (error rates, RTs, and RT slopes) and the level of hypothetical attentional subprocesses (STRAVIS focus size, dwell time, and movement time).

Assessment of Predictor Selection

In the left panels of Figure 5, the empirical mean of patients classified as unimpaired and that of controls are marked by two different horizontal lines. Their differences provide the centers of the 90% confidence intervals for the theoretical difference of means, which is zero if the model holds. The intervals are shown in Table 3. For all six DMs, the empirical mean of patients classified as unimpaired was larger than that of controls. However, in neither case, this difference was significant at level $\alpha = .10$ (the 90% confidence interval for the theoretical difference contained the 0). Because the degrees of freedom of the t fractions for the six DMs were quite large (50, 36, 34, 36, and 37, respectively), the possibly insufficient power is less likely a result of insufficient sample size but of effects being small. It might indicate that most patients in the "unimpaired" group are truly unimpaired, but not all, so a slightly different choice of predictors would possibly yield a similar picture. Indeed, for four of the six DMs, predictor selection was also confirmed for the second-best model when using 90% confidence intervals. The best models came out superior in five of the six DMs (except STRAVIS movement time) only when comparing the precise significance levels of the t tests. In

Figure 5. Left panels: Distribution of the six DMs in (A–F) patients ($n = 28$) and controls ($n = 28$). Patients were split up into subgroups according to their lesions determined as crucial for each DM ("prediction levels"). In the subgroup with zero lesions, the unfilled dots represent the data of the control subjects, with two horizontal lines indicating the sample means of controls and "unimpaired" patients. The dotted curves show the theoretical distribution as estimated from the LM fit of the DMs. The middle and right panels show the data of the second sample of controls ($n = 12$) and patients ($n = 12$) used for model validation. The .90 prediction intervals for the sample mean (controls) and for individual data (patients) are marked in gray. The lighter gray intervals give the latter with Bonferroni-adjustment. For details, see the Appendix A.

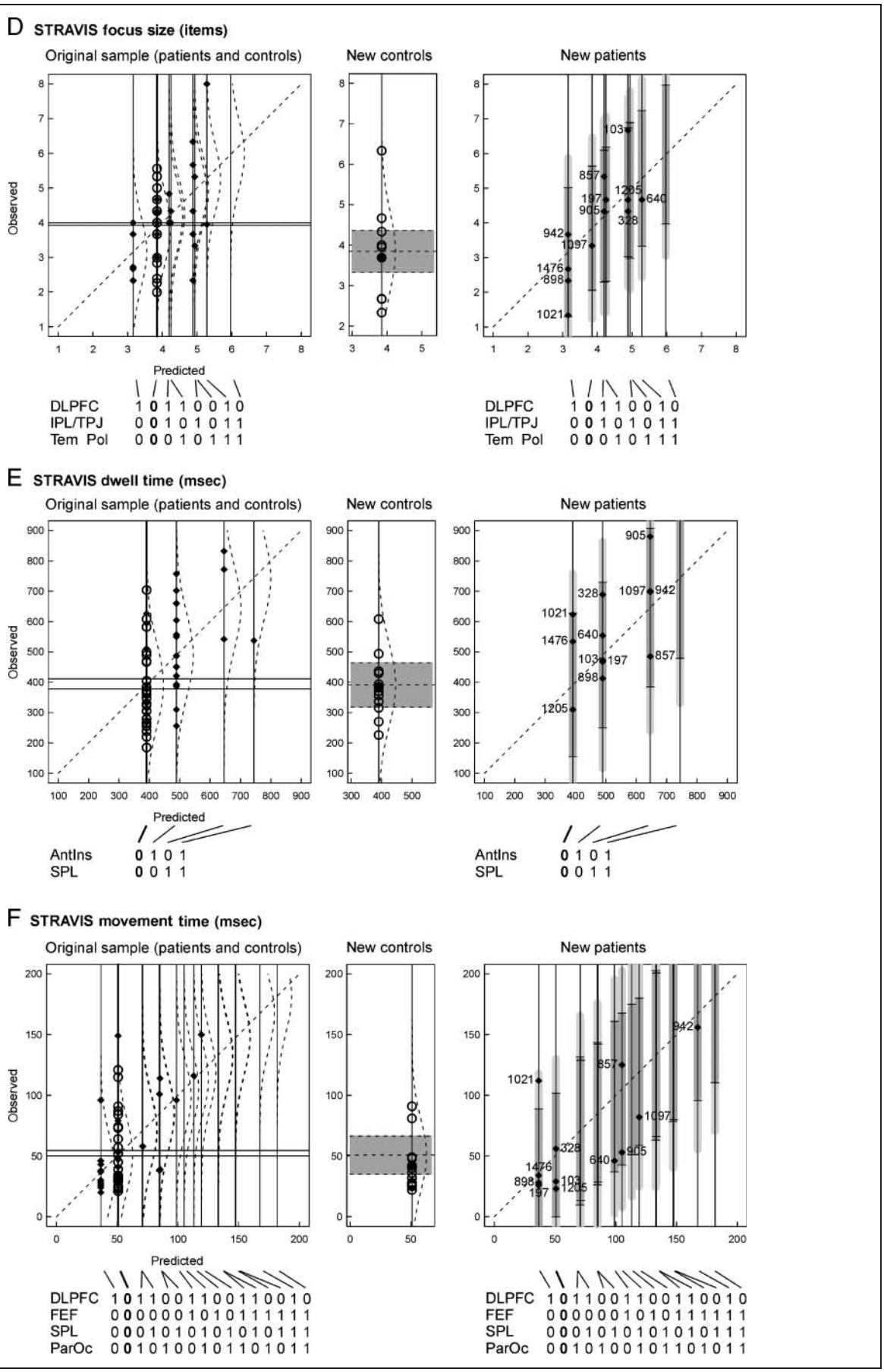

Figure 5. (*continued*)

Table 4. Validation Sample: Gender, Age, Main Etiology of Lesion(s), Affected Brain Area(s), Lateralization, Time Interval between Lesion Event and Testing, Distribution of Lesion, and Further Pathologies

No	*Gender*	*Age*	*Etiology*	*(1) DLPFC*	*(2) FEF*	*(3) AntIns*	*(4) IPL/TPJ*	*(5) TPol*	*(6) SPL*	*(7) ParOc*	*LH*	*RH*	*Dist*[a]	*Size*[b]	*Further Pathologies*
103	f	62	Infarction	0	0	1	1	0	0	0	1	0	0	1	Left BG
197	f	60	ICB	1	0	1	0	1	0	0	1	1	0	0	Bil CC, BG, VLPFC
328	m	46	Infarction	0	0	1	1	0	0	0	0	1	0	1	(unc. fasc.)
640	m	59	Infarction	1	1	1	1	1	0	0	0	1	0	1	Right VLPFC
857	m	57	Infarction	1	0	0	1	0	1	1	1	1	1	0	Bil VLPFC
898	m	57	Infarction	1	0	1	0	0	0	0	1	0	0	1	Left unc. fasc., VLPFC
905	m	52	Infarction	1	0	0	1	0	1	1	1	0	1	1	Left VLPFC
942	f	42	CNS vascular	1	1	0	0	0	1	1	1	1	1	0	Bil VLPFC
1021	m	38	Tumor OP	1	0	0	0	0	0	0	1	0	0	0	Fronto-polar, left VLPFC
1097	m	58	Infarction	0	0	0	0	0	1	1	0	1	1	0	
1205	m	53	AVM	0	0	0	1	0	0	0	1	0	0	0	
1476	m	39	Tumor OP	1	0	0	0	0	0	0	0	1	0	0	Right VLPFC
n				8	2	5	6	2	4	4	8	7	4	5	

AntIns = anterior insula; TPol = temporal pole; ParOc = parieto-occipital; TBI = traumatic brain injury; ICB = intracerebral bleeding; AVM = arteriovenous malformation; LH = left hemisphere; RH = right hemisphere; WM = White matter; BG = basal ganglia; thal = thalamic nuclei; VLPFC = ventrolateral prefrontal cortex (inferior frontal gyrus); unc. fasc. = uncinate fasciculus.

[a]Distribution of lesion: 0 = unifocal, 1 = multifocal.

[b]Size: 0 = small, 1 = large according to expert rating.

sum, no model was rejected because of predictor selection, but the use of 90% confidence intervals (significance level $\alpha = .10$) did not seem particularly sensitive for assessing every single predictor.

Assessment of Variance Explanation Achieved by the Models

For the observed measures error rate, RT, and RT slope, the 90% confidence intervals for the theoretical variance ratio did not contain the 1 (see Table 3); the residual variance in patients ($\hat{S}^2_{Res,p}$) was thus significantly greater than the variance in controls ($\hat{S}^2_c$) at $\alpha = .10$. This lets us conclude that in none of the three cases the model explained the data satisfactorily (for error rate, $\frac{\hat{S}^2_{Res,p}}{\hat{S}^2_c}$ was 6.67; for RT, we obtained $\frac{\hat{S}^2_{Res,p}}{\hat{S}^2_c} = 4.7$; and for the RT slope, we found $\frac{\hat{S}^2_{Res,p}}{\hat{S}^2_c} = 2.09$[6]). In contrast, for the three hypothetically underlying measures STRAVIS focus size, dwell time, and movement time, the residual variance in patients did not significantly ($\alpha = .10$) differ from the control variance. More precisely, the respective empirical variance ratios and F tests yielded $\frac{\hat{S}^2_{Res,p}}{\hat{S}^2_c} = 1.52$ ($p = .30$) for the focus size, $\frac{\hat{S}^2_{Res,p}}{\hat{S}^2_c} = 1.38$ ($p = .42$) for the dwell time, and $\frac{\hat{S}^2_{Res,p}}{\hat{S}^2_c} = 1.22$ ($p = .62$) for the movement time. Accordingly, we here regarded the portion of variance explained by the lesions satisfactory. For all six DMs, the second-best models yielded a larger variance ratio and a lower p value than the best ones and proved thereby inferior. It seems further noteworthy that the absolute value of the explained portion of variance R^2 (Table 3) did obviously not reflect its "goodness."

Validation of Model Intercept with a New Control Sample

For all DMs but error rate, the sample mean of the new control sample met with its .90 prediction interval constructed around the model intercept $\hat{\beta}_0$ (see the middle panels of Figure 5 and Table 3). The same was true for the second-best models (which does not surprise, given that the intercepts were estimated very similar). Thus, the estimated intercept values were validated in all cases except for error rate.

Model Validation with a New Patient Sample

For each of the six DMs, we compared the data of the patients of the new sample with the values predicted from

their lesions according to the above LMs. The right-hand panels in Figure 5 plot the two sets of values against each other. The diagrams resemble those of the original sample as shown in the left-hand panels of the figure except that the theoretical distributions are left out. In each, the dotted line shows the theoretical position of mean predictions if the model held. Around this, the .90 prediction intervals for the single data and the Bonferroni-adjusted .90 prediction intervals for $n = 12$ are depicted (see Methods section and Appendix A). In the last column of Table 3, it is summarized for each model how many of the $n = 12$ observations were within their .90 prediction interval and whether all 12 observations were within their Bonferroni-adjusted intervals. If the latter was not the case, the validation was considered failed. For error rate as well as RT and RT slope, the observed values did obviously not agree well with the predictions. For error rate, the correlation between predictions and observations was even slightly negative (Figure 5). Note that here, probably because of the large portion of unexplained variance, the Bonferroni prediction intervals were not sensitive enough for indicating the failure. For the RT slope, predictions were better than for the absolute RT but obviously still not satisfactory. The diagram in Figure 5 suggests that in particular three or four patients, Patients 1021, 857, 942, and possibly 103, were not adequately treated by the model. Patient 1021 had a single but large lesion to the DLPFC and was clearly slowed in visual search time and efficiency. Neither the RT nor the RT slope model covered DLPFC lesions. The same might apply to Patient 942. On the other hand, Patient 857 had bilateral lesions, which included the DLPFC, the IPL/TPJ, the SPL, and the parieto-occipital cortex. His search time was on average normal but faster in displays with eight than with four or six items, leading to a negative slope. Because his parieto-occipital lesion should, according to the model, enhance the slope, it was grossly overestimated by the model. A similar problem might apply to Patient 103, who had a single insular lesion which should, according to the model, lead to an enhanced RT slope, that is, reduced efficiency in standard visual search terms. But contrary to prediction, her slope was normal (or even reduced).

For the three STRAVIS parameters, the picture was different: As the diagram in Figure 5 shows, the patients with a lesion to the DLPFC had, as predicted, on average a reduced focus size, whereas in patients with temporal lesions, the average focus size was enlarged. All 12 observed patient values fell into their .90 prediction intervals. The model was thereby validated.

The STRAVIS dwell time was assumed to rise with insular and parietal (SPL) lesions. This model was also validated in the new sample: The mean dwell times were quite accurately predicted, as again every single observation was within its .90 interval.

The STRAVIS movement time in the new sample was, as predicted, on average prolonged with FEF and parietal lesions and reduced with DLPFC lesions (with the exception of Patient 1021). Accordingly, 11 of the 12 observations were within their .90 prediction interval. Because the Bonferroni intervals covered all observations, we did not reject the model. It further seems particularly noteworthy that the only new patient with all three crucial lesions (FEF, SPL, parieto-occipital) had, as predicted, the longest STRAVIS movement time.

For all six DMs, the models originally classified as second-best ones came out worse with the new sample as well (Table 3), thereby confirming the original ranking.

Exploring Further Sources of Variance

Additional Predictors

Beside the seven brain areas coded here, there were further brain pathologies present in some of the patients. The contribution of BG (Fimm et al., 2001) and of thalamic nuclei (Soto, Humphreys, & Rotshtein, 2007; Robinson & Petersen, 1992; Crick, 1984) to visual search has been repeatedly stated in the literature. We thus ran the linear modeling algorithm (see Methods section) again with these two lesion areas as additional predictors. First, we found that with nine predictors, the sequences of subsets selected for each subset size (one, two, etc., predictors) were not ordered anymore, indicating the solutions not being as robust as above. Although it goes without saying that R^2 of the full model was larger with nine than with seven predictors, the finally preferred subsets and models were identical to the ones originally favored in all cases. In particular, for the STRAVIS dwell time, the two additional predictors added almost nothing.

Not only anatomical sites but also other lesion parameters like the distribution (whether there were one or more foci), the size, or the time since the lesion event might affect the cognitive processes under investigation. The pairwise associations between these variables and the six DMs were mostly weak. However, they might reveal their influence only in combination with other predictors, in particular by moderating the effect of the anatomical site of a lesion. In linear modeling, moderator effects are expressed by including interaction terms in the model equation. This is explored in the following.

Nonlinear Relations

The effects of lesions to the various brain areas have been treated as additive so far. However, it seems much more plausible that the interplay between different lesion areas is more complex. For example, subcortical structures like BG or thalamic nuclei might possibly not supply independent contributions but rather subserve mediating functions in communicating attention-related signals in the brain (Soto et al., 2007; Robinson & Petersen, 1992; Crick, 1984). A lesion to such a mediating structure would then attenuate or even annihilate the effect of a lesion to the primary structure. A similar case probably holds for the

lesion lateralization as additional (moderating) variable and for nonanatomical factors like the size of a lesion, which might moderate the influence of the above lesions rather than add a constant amount to their effect. In the same way, the lesion areas already selected as relevant predictors might not act in a simple additive way but rather interact themselves.

Statistically, this can be addressed by including interaction terms in the LM and by running the exhaustive predictor selection algorithm as above and see whether interaction terms remain in the favored subset of predictors. Our sample was much too small to do this exhaustively, that is, to include all interactions between the seven (or nine) lesion sites and the three nonanatomical variables as predictors, because with the inclusion of every moderating variable, the number of predictors is doubled. However, we explored the notion by starting from the predictor subsets chosen above and examined pairwise interactions between the selected areas and (1) each of the other selected areas, (2) the BG and thalamic lesions, and (3) the lesion size (binary-coded) according to two independent expert ratings (0 = *small*, 1 = *large*). Models of Types 1–3 were run independently. With three "primary" predictors, Types 1 and 3 resulted in a six-predictor model for start and Type 2 resulted in a nine-predictor model. From this set of predictors, we choose the best subset with the algorithm described above and, if different from the original model, applied the validation procedure (comparison of residual variance with control group variance and comparison of "observed" with predicted values in the second patient sample; see Methods section). Although in some cases the inclusion of interaction terms yielded models that explained more variance (e.g., R^2 = .68 instead of .54 in case of RT, and R^2 = .33 instead of .28 in case of the STRAVIS movement time), in neither case predictions in the new samples were improved. In a similar way, it could in principle be tested whether the hemisphere of a lesion had an impact. Because for each structure, two interaction terms need to be added; this has to be left to future studies with larger samples.

DISCUSSION

Summary of Results

Patients with visuospatial attention problems after diverse focal lesions to the frontal, temporal, and/or parietal lobe showed impaired performance in a visual feature search task with graded target-distractor similarity compared with age-matched controls. They searched only marginally less accurately but significantly more slowly and less efficiently. When exploring the nature of this difference by decomposing the RT into the times of hypothetical subprocesses of the task according to the STRAVIS model (Müller-Plath & Pollmann, 2003), we found prolonged estimated dwell times as well as prolonged estimated movement times of attention. The core parameter of STRAVIS, the size of the attentional focus, did not significantly differ between patients and controls.

We then applied LMs to the patient data to identify those brain lesions that were most predictive for the two observed measures error rate and RT and the standard measure of search efficiency, RT slope, as well as for the three hypothetical measures STRAVIS focus size, dwell time, and movement time and to quantify their contribution. For each measure, a subset of lesion areas was selected as (binary) predictors so that a minimum number of predictors explained a maximum portion of variance. The error rate was best linearly modeled by temporopolar lesions as sole predictor. However, with an independent patient sample, the model could not be validated. The picture was not much better for the RT: Although the best LM, which predicted the RT from insular, parietal, and parieto-occipital lesions, accounted for a large portion of the variance, the estimated effects of these lesions were not validated by the second sample. The RT slope was best predicted by insular, parieto-occipital, and temporopolar lesions, the latter reducing the slope. Here, predictions for the second sample were better but still not satisfactory in every detail. We conclude that it was not possible to satisfactorily predict the global behavioral measures of the task by a linear combination of the brain lesion areas under investigation. Including interaction terms into the LMs did not change results. One has to keep in mind that the same slope can result from few long-lasting search steps as well as many fast steps. With the model STRAVIS, it is possible to tell the two patterns apart.

Indeed, the picture changed when we modeled measures of the hypothetically underlying attentional subprocesses: The STRAVIS focus size, although not differing between the patients in total and controls, depended strongly on the site of lesion. Patients with a DLPFC lesion selected on average—according to STRAVIS—less items into their focus compared with controls, whereas in patients with temporal lesions (IPL/TPJ as well as temporal pole), the focus size was enhanced. It might be interesting to note here that temporal pole lesions were, although not validated in the second sample, also predictive for an enhanced error rate. Under certain circumstances, an enlarged focus size might therefore be as detrimental as a reduced one. The residual variance was comparable to that of controls, and the LM was validated with the second patient sample. A similarly good explanation of variance was achieved when predicting the other two attention-related STRAVIS model parameters linearly from the presence of lesions in the investigated brain areas. Most predictive for the dwell time were lesions to the anterior insula and the SPL, whereas the movement time was best predicted by lesions to the FEF, to the SPL, and to the parieto-occipital cortex, each enhancing the movement time. Again, the residual variance was comparable to that of controls, and the data

of the second sample agreed with the model. Again, including additional predictors or nonlinear relations did not improve the models.

The Attentional Focus Size Is Predicted by Lesions to the DLPFC and the Temporal Lobe

After specifying the relations between hypothetical cognitive subprocesses and STRAVIS parameter values, abnormal parameter values can be interpreted according to STRAVIS model assumptions (see the Methods section). A reduced focus size might result from perceptual feature processing being ineffective, so that saliency maps are less informative, or from attentional control processes being impaired, so that anticipative top–down adjustment of the focus size is hampered. The latter might as well result in an inadequately large focus.

Although neural correlates of the attentional focus size have been well documented in retinotopic visual areas (Müller, Bartelt, Donner, Villringer, & Brandt, 2003; Brefczynski & DeYoe, 1999), much less is known about the areas which control attentional size changes. Adjustment of the attentional focus size has been indirectly linked to the temporal lobes by the finding that deficits in focus size adjustments were observed in nondemented carriers of the ε4-allele of the apolipoprotein E gene, which is a risk factor for dementia of the Alzheimer's disease (AD; Greenwood, Sunderland, Friz, & Parasuraman, 2000). The same deficit has been observed in patients with AD (Greenwood, Parasuraman, & Alexander, 1997). Because temporal cortex is affected earliest by the neuropathology of AD (Braak & Braak, 1991), the link between apolipoprotein E ε4-carriers and focus size adjustment may be due to early, subclinical, temporal processing deficits.

Dorsolateral prefrontal activation during divided attention has been reported (Corbetta, Miezin, Dobmeyer, Shulman, & Petersen, 1991). This may be seen as a special case of a large attentional focus. In agreement with this, a recent imaging study observed lateral prefrontal activation (BA 46) when the attentional focus was enlarged, whereas during "zooming in" to a smaller focus activation along, the anterior intraparietal sulcus was observed (Chen, Marshall, Weidner, & Fink, 2009). This observation as well as the stronger lateral prefrontal activation for divided versus selective attention (Corbetta et al., 1991) fits quite nicely with our finding of a small focus in patients with DLPFC lesions. It may thus be that lateral prefrontal cortex supports not focus changes in general but particularly enlarging of the attentional focus, leading to an inadequate small focus in our DLPFC patients.

The Attentional Dwell Time Is Predicted by Lesions to the Anterior Insula and the SPL

The STRAVIS dwell time will be prolonged if attentional modulation of perception is ineffective, if perceptual comparison of features is impaired, or if decision making is slowed. To our knowledge, the neuronal correlate of the attention dwell time has not been directly investigated previously.

Attentional modulation of feature perception mainly involves occipital visual areas (see, e.g., Kastner, DeWeerd, Desimone, & Ungerleider, 1998), which were not investigated here. The concept of the attentional dwell time is further related to sensory decision making. Attention dwells on a part of the search display until the observer makes a decision about target presence or absence in the attended area. Ramp-like neuronal responses, which may reflect the accumulation of evidence needed to make a sensory decision, have been found in area LIP (Shadlen & Newsome, 1996) as well as in DLPFC (Kim & Shadlen, 1999) of nonhuman primates. One can further ask what kind of processes may subserve these target decisions in parietal and frontal cortex. Specifically in visual search, attentional capture by salient stimuli is reduced by repetitive TMS over posterior parietal cortex (Hodsoll, Mevorach, & Humphreys, 2009). The intact SPL further supports inhibition of distractors (Pollmann et al., 2003). Thus, both facilitatory and inhibitory mechanisms, which guide attention to the target in a search display, are disrupted after superior parietal lesions. This, in turn, will result in prolonged dwell times needed to make a decision about target presence in a currently attended part of the search display and about the landing position of the next saccade.

Recently, we conducted an fMRI study of STRAVIS (Müller-Plath, 2008) in which we applied the same search task as in the present study and correlated BOLD signal changes with STRAVIS dwell time and movements across the different task conditions within each individual. Beside lateral occipital activations, we found the right anterior insula correlating with the dwell time, a finding that was repeated here.

Our recent eye movement data (Heße et al., submitted) showed that the dwell time is overestimated in individuals who often return to previously visited items during their search. Damage to the right intraparietal sulcus or right inferior frontal cortex may lead to pathological forgetting (and consequently revisiting) of previously visited items during search (Mannan et al., 2005). This may have contributed to the high dwell time estimates for SPL lesions (Figure 5). An updated model version STRAVIS 2.0 that distinguishes dwell times and number of reinspections is currently being developed (Müller-Plath, Heße, Melzer, & Wienrich, in preparation).

The Attentional Movement Time Is Predicted by Lesions to the DLPFC, FEF, and Parietal Cortex

A prolonged movement time indicates difficulties in disengaging attention, possibly resulting from computation of spatial coordinates for the movement ("where") being ineffective or from saccade initiation being disturbed ("when"; see Findlay & Walker, 1999).

It is no surprise that FEF lesions led to increased movement times because the FEF is a central structure for the guidance of eye movements as well as covert attention shifts. The FEFs contain a visual salience map, in the sense that neuronal responses reflect the behavioral significance of the stimuli in a visual scene, independent of whether an overt eye movement is carried out or not (Juan et al., 2008; Thompson & Bichot, 2005). Neurophysiological evidence (Monosov, Trageser, & Thompson, 2008) suggests that in the noninjured brain, the FEF is central for the selection of the target location in visual search. Spatially specific microstimulation of FEF neurons leads to spatially specific activations in V4 (Moore & Armstrong, 2003) and lowers target detection thresholds (Moore & Fallah, 2004). Consequently, interruption of neuronal activity in human FEF by TMS, which can serve as a reversible "lesion model," leads to impaired visual search performance (O'Shea, Muggleton, Cowey, & Walsh, 2004). The spatially specific functional connectivity between V4 and visual areas (Armstrong & Moore, 2007; Moore & Armstrong, 2003) fits well with our finding that, in addition to FEF lesions, parieto-occipital lesions also affected movement times. The third area for which our model implies prolonged movement times, when lesioned, posterior parietal cortex, is intricately connected to the FEF on the one hand and visual cortex on the other hand and is well known to be vital for spatial computation (Lewis & van Essen, 2000; Wise, Boussaoud, Johnson, & Caminiti, 1997). Moreover, many experimentally similar studies on humans report a right DLPFC activation: Pollmann and von Cramon (2000), for example, found DLPFC activation associated with visual search difficulty and proposed a role in voluntary control of visuospatial orienting. Our own fMRI study on a very similar task as used here (Müller-Plath, 2008) corresponded well with the present results in showing movement related activation in the (right) DLPFC, FEFs, SPL, descending IPS, and IPS/TOS.

Modeling Subprocesses of Attention with STRAVIS

Interestingly, the focal brain lesions were only predictive for the STRAVIS model parameters but not for the global measures of visual search performance like error rate or RT. The standard measure of search efficiency, the RT slope, was not fully satisfactorily predicted either. The four patients mentioned above (Patients 1021, 857, and 103) who apparently caused rejection of the RT slope model might illustrate the advantage of decomposing visual search into hypothetical subprocesses: A flat (or even negative) slope can either result from dwell and movement times being extremely fast or from the focus being abnormally large. If the latter is coupled with dwells and/or movements being abnormally slow, the absolute RT will be large, so the search should be regarded impaired, in spite of the flat slope, which suggests high efficiency in standard terms. According to STRAVIS, this applied to Patients 103 and 857 (see Figure 5). The LMs attributed the enlarged focus to the temporal lesions and the slowed dwell (Patient 103) and movement (Patient 857) time to the insular and parietal lesions of the respective patients. On the other hand, the high RT slopes of Patients 1021 and 942 were, according to STRAVIS, the result of an abnormally small focus, which was, according to the LM, due to the DLPFC being lesioned. The only result not covered by the models was the movement time of Patient 1021 being prolonged and not reduced, as predicted from his DLPFC lesion. One might consider dropping DLPFC as predictor here. However, the three-predictor model of the movement time came out slightly worse in the original as well as the validation sample, as did a different choice of a fourth predictor (see Table 3). Although Patient 1021 might be atypical for some reason, the role of DLPFC lesions for the movement time might be worth further investigation.

In sum, this supports the notion that in studying relationships between structure and function in the brain, it is necessary to have a sufficiently fine-grained description of the function. We would like to suggest that the STRAVIS parameters focus size, dwell time, and movement time reflect cognitive subprocesses at a level fine enough to be associated with (a set of) different anatomical brain structures. The focus size hypothetically reflects the efficiency of attentional modulation of feature perception, resulting in more or less informative saliency maps. Control and execution of this modulation both contribute to its efficiency. The STRAVIS dwell time depends on the efficiency of attentional modulation of feature perception as well as on perceptual decision making. The movement time should reflect the speed of disengaging attention, possibly resulting from how fast spatial coordinates for the movement ("where"; see Findlay & Walker, 1999) are computed and—in overt search—the speed of saccade initiation ("when"; see Findlay & Walker, 1999).

Linearly Modeling the Effects of Various Brain Lesions

In the past, effects of focal lesions have mostly been studied in separation of each other. However, this is a problem if the patients, as is often the case, have other lesions apart from the one under investigation. The problem is nicely illustrated if one compares the effects of lesion areas taken separately (Figure 4) to the predictor selection in the best LMs (Table 3, Figure 5): Not always were the lesions with the largest effects selected as relevant predictors. For example, DLPFC lesions had, taken separately, almost no obvious effect on the STRAVIS dwell time. Nevertheless, they explained more additional variance when combined with SPL and parieto-occipital lesions than any other predictor. This illustrates the effect of predictor intercorrelations in linear modeling (also known as "suppressor effects" in regression): By adding a predictor that is uncorrelated with the criterion but not with the other predictors, the predictor space may be expanded in such a way that the distance from the

criterion vector to the predictor space is reduced, corresponding to the portion of explained variance being enhanced. Because the presence of a DLPFC lesion was negatively correlated to the presence of an SPL lesion (see Table 2), it has obviously acted in such a way (for details on this very clear and instructive geometrical description of LMs, see Wickens, 1995).

A simple type of LMs, which was applied here, is combining predictors additively. However, with the same rationale, it is possible to model the effect of predictor interaction by including multiplicative terms. Even more complex relationships between predictors can be incorporated, using, for example, generalized LMs. One problem here is that theories on structure–function relationships are probably not elaborated well enough to distinguish between concurrent model types. Second, the sample size necessary to obtain a stable fit increases exponentially with the number of predictor terms. However, the present study demonstrates that at least the simplest type of models runs successfully on a small sample. The models that used only additive predictor combinations yielded unequivocal and stable solutions (Table 3).

Conclusions

The linear modeling approach seems a promising new approach in studying the neural basis of complex cognitive processes. In the present study, we described visual search with the help of the RT model STRAVIS (Müller-Plath & Pollmann, 2003) and applied LMs to predict the effect of diverse focal brain lesions onto the model parameters. Even with a quite small sample like ours, interesting results could be reached: Critical lesion areas for the STRAVIS focus size were the DLPFC, the inferior parietal lobe including the TPJ (IPL/TPJ), and the temporal pole, with DLPFC lesions reducing the focus and temporal lesions enlarging it. The STRAVIS dwell time was reduced in patients with anterior insular and SPL lesions. Lesions to the FEFs, the SPL, and the parieto-occipital cortex were most detrimental to the STRAVIS movement time. All findings were validated with an independent sample. This was not the case when we tried to predict the global behavioral measures error rate, RT, or RT slope from the location of the lesions.

We concluded that structure–function relationships can be studied successfully only if a sufficiently fine-grained description of the function is obtained. Here, our results provide further support to the STRAVIS model, that is, further evidence that the task indeed consists of the hypothesized subprocesses, and that the individually estimated parameter values reflect their efficiency.

The visual search task and the STRAVIS model might therefore be applied as a process-oriented diagnostics of impairments of visuospatial and selective attention. On the basis of such a process-oriented diagnostics, therapeutic measures might be individually optimized to improve the individually impaired subprocess.

APPENDIX A

Linear Model with *m* Binary Predictors

Suppose that $\mathbf{x_{(k)}}$ are binary variables ("predictors") and Y is a metric random variable (DM). By building all possible m-tuples prom the predictor values 0 and 1, 2^m different predictor values can be defined: For $k = 1, \ldots, 2^m$, let the predictor vector at level k be $\mathbf{x_{(k)}} = (x_{(k)1}, \ldots, x_{(k)m})$ so that $x_{(k)j} \in \{0, 1\}$, $\mathbf{x_{(k)}} \neq \mathbf{x_{(l)}}$ for $k \neq l$ and that the $\mathbf{x_{(k)}}$ vectors are in lexicographic order. The population of subjects is thereby partitioned into 2^m subpopulations $\Omega_{(k)}$.

For a given sample of n subjects, n_k of which are from subpopulation $\Omega_{(k)}$ (with $0 \leq n_k \leq n$), let

$$\mathbf{Y} = \begin{pmatrix} Y_1 \\ . \\ . \\ Y_n \end{pmatrix}, \mathbf{X} = \begin{pmatrix} 1 & x_{11} & \ldots & x_{1m} \\ . & . & . & . \\ . & . & . & . \\ 1 & x_{n1} & \ldots & x_{nm} \end{pmatrix}, \text{ and}$$

$$\boldsymbol{\beta} = \begin{pmatrix} \beta_0 \\ \beta_1 \\ . \\ \beta_m \end{pmatrix},$$

where $\mathbf{X}$ is the $n \times (m + 1)$ design matrix in which n_k rows correspond to the predictor vector $\mathbf{x_{(k)}}$, $\boldsymbol{Y}$ is the n-dimensional random variable the components of which are drawn from the respective subpopulations, and $\boldsymbol{\beta}$ is a $(m + 1)$-dimensional parameter vector. Suppose that $\mathbf{X}$ has full rank. An LM for $\mathbf{X}$ and $\mathbf{Y}$ with parameter β holds if $E(\mathbf{Y}) = \mathbf{X}\,\boldsymbol{\beta}$ and $\boldsymbol{Y} \sim N_n(\mathbf{X}\,\beta, \sigma^2\,\mathbf{I})$. The least squares estimator for $E(\mathbf{Y})$ is given by $\hat{\boldsymbol{Y}} = \mathbf{X}\hat{\boldsymbol{\beta}}$ with $\hat{\boldsymbol{\beta}} = (\mathbf{X}'\mathbf{X})^{-1}\mathbf{X}'Y$, the sampling distribution of which is

$$\hat{\boldsymbol{\beta}} \sim N_{m+1}\left(\boldsymbol{\beta}, \sigma^2(\mathbf{X}'\mathbf{X})^{-1}\right). \tag{A1}$$

Because the DM is distributed identically within subpopulations, let $Y_{(k)}$ denote the n_k identical random variables Y_i corresponding to a predictor level k that is present in the design matrix $\mathbf{X}$. For the predictor vector $\mathbf{x_{(k)}}$, the LM may be written as

$$Y_{(k)} \sim N\left(\mu_{(k)}, \sigma^2\right) \quad \text{with} \quad \mu_{(k)} = (1, \mathbf{x_{(k)}})\boldsymbol{\beta} = \beta_0 + \sum_{j=1}^{m} \beta_j\, x_{(k)j}, \tag{A2}$$

and the prediction is

$$\hat{Y}_{(k)} = (1, \mathbf{x_{(k)}})\hat{\boldsymbol{\beta}} = \hat{\beta}_0 + \sum_{j=1}^{m} \hat{\beta}_j\, x_{(k)j}. \tag{A3}$$

Within-sample Validation

Confidence Interval for Assessing Whether "Unimpaired" Patients Have the Same Mean as Controls

Suppose that in the design matrix $\mathbf{X}$, the subsample with predictor vector $\mathbf{x_{(1)}} = (0, \ldots, 0)$ consists of n_c controls

plus n_0 patients ($n_c + n_0 = n_1$). The patients at this level are classified as unimpaired because none of the m brain lesions determined as relevant were present in them. Let M_c denote the sample mean in the n_c controls, M_0 the sample mean in the n_0 patients, and $\hat{S}_c^2$, $\hat{S}_0^2$ the respective (unbiased) sample variances. If the LM (equation A2) holds, then M_c and M_0 are independent estimators of $\mu_{(1)}$. Further, $\hat{S}^2_{\text{pooled}} = \frac{(n_0-1)\cdot\hat{S}_0^2+(n_c-1)\cdot\hat{S}_c^2}{n_0+n_c-2}$ is an unbiased estimator of the error variance σ^2 and the limits of the $(1 - \alpha) \times 100\%$ confidence interval for the difference of the expected subsample means $E(M_c) - E(M_0) = \mu_{(1)} - \mu_{(1)} = 0$ are (see, e.g., Hays, 1994, p. 327)

$$M_0 - M_c \pm t_{n_0+n_c-2;\alpha/2} \cdot \hat{S}_{\text{pooled}} \cdot \sqrt{\frac{n_0+n_c}{n_0 \cdot n_c}}. \qquad \text{(I.i)}$$

(The numbering of intervals refers to the numbering in the main text.)

Confidence Interval for Assessing Whether the Residual Variance in Patients Is Identical to the Variance in Controls

Let $\hat{S}_c^2$ denote the (unbiased) sample variance of the n_c controls and $\hat{S}^2_{\text{Res},p} = \frac{1}{n_p-m-1}\cdot\sum_{i=1}^{n_p}(Y_i - \hat{Y}_i)^2$ the residual variance of the n_p patients when fitting the LM. If the above assumption (equation A2) holds, then $\hat{S}_c^2$ and $\hat{S}^2_{\text{Res},p}$ (as random variables) are independent estimators of σ^2, the ratio of which is distributed as $F_{n_c-1,\,n_p-m-1}$ (see, e.g., Hays, 1994, p. 360). The (asymmetrical) $(1 - \alpha) \times 100\%$ confidence interval for the ratio of expected subsample variances $\frac{E(\hat{S}_c^2)}{E(\hat{S}^2_{\text{Res},p})} = \frac{\sigma^2}{\sigma^2} = 1$ is then given by

$$\left[\frac{\hat{S}^2_{\text{Res},p}}{\hat{S}_c^2}\cdot F_{n_c-1,n_p-m-1;1-\alpha/2},\ \frac{\hat{S}^2_{\text{Res},p}}{\hat{S}_c^2}\cdot F_{n_c-1,n_p-m-1;\alpha/2}\right]. \qquad \text{(I.ii)}$$

Cross Validation

Prediction Interval for Assessing Whether the LM Holds for a New Subject at Level k′

Suppose that an LM fit was obtained for a sample with design matrix $\mathbf{X}$. Suppose further that $\mathbf{x}_{(\mathbf{k}')} = (\mathbf{x}_{(\mathbf{k}')1}, \ldots, \mathbf{x}_{(\mathbf{k}')m})$ is the (binary) predictor vector of any new subject with DM $Y_{(k')}$. Note that $\mathbf{x}_{(\mathbf{k}')}$ need not necessarily correspond to any predictor vector in the design matrix $\mathbf{X}$. In this case, however, we assume that the LM (equation A2) holds for $\mathbf{x}_{(\mathbf{k}')}$, too:

$$Y_{(k')} \sim N(\mu_{(k')}, \sigma^2) \quad \text{with} \quad \mu_{(k')} = (1, \mathbf{x}_{(\mathbf{k}')})\boldsymbol{\beta} = \beta_0 + \sum_{j=1}^{m}\beta_j x_{(k')j}. \qquad \text{(A2′)}$$

Further, we use the parameter estimator $\hat{\boldsymbol{\beta}}$ from the original sample for predicting $Y_{(k')}$:

$$\hat{Y}_{(k')} := (1, \mathbf{x}_{(\mathbf{k}')})\hat{\boldsymbol{\beta}} = \hat{\beta}_0 + \sum_{j=1}^{m}\hat{\beta}_j x_{(k')j}. \qquad \text{(A3′)}$$

To construct an interval around $\hat{Y}_{(k')}$ in which $Y_{(k')}$ lies with probability $1 - \alpha$ if the equations A2 and A2′, respectively, are true, the distribution of the difference variable $U := Y_{(k')} - \hat{Y}_{(k')}$ under this assumption is required.

Because of equation A2/A2′, the new observation $Y_{(k')}$ is normally distributed with expectation $E(Y_{(k')}) = (1, \mathbf{x}_{(\mathbf{k}')})\,\boldsymbol{\beta}$ and variance $V(Y_{(k')}) = \sigma^2$.

Because of equation A3/A3′ and equation A1, the prediction $\hat{Y}_{(k')}$ is normally distributed with expectation $E(\hat{Y}_{(k')}) = E\big((1, \mathbf{x}_{(\mathbf{k}')})\hat{\boldsymbol{\beta}}\big) = (1, \mathbf{x}_{(\mathbf{k}')})E\big(\hat{\boldsymbol{\beta}}\big) = (1, \mathbf{x}_{(\mathbf{k}')})\boldsymbol{\beta}$ and variance $V(\hat{Y}_{(k')}) = V((1, \mathbf{x}_{(\mathbf{k}')})\hat{\boldsymbol{\beta}}) = (1, \mathbf{x}_{(\mathbf{k}')})V(\hat{\boldsymbol{\beta}})(1, \mathbf{x}_{(\mathbf{k}')})' = \sigma^2(1, \mathbf{x}_{(\mathbf{k}')})(\mathbf{X}'\mathbf{X})^{-1}(1, \mathbf{x}_{(\mathbf{k}')})'$.

With $Y_{(k')}$ and $\hat{Y}_{(k')}$ being random variables on different populations and thereby independent, it follows that U is normally distributed with

$$E(U) = E(Y_{(k')}) - E(\hat{Y}_{(k')}) = 0 \quad \text{and}$$

$$V(U) = V(Y_{(k')}) + V(\hat{Y}_{(k')}) = \sigma^2(1 + (1, \mathbf{x}_{(\mathbf{k}')})(\mathbf{X}'\mathbf{X})^{-1}(1, \mathbf{x}_{(\mathbf{k}')})')$$

(see also Fox, 1997, p. 234). Because the residual variance $\hat{S}^2_{\text{Res}} = \frac{1}{n-m-1}\sum_{i=1}^{n}(Y_i - \hat{Y}_i)^2$ from the original model fit is an unbiased estimator of σ^2, the $(1 - \alpha)$ prediction limits for $\hat{Y}_{(k')}$ are given by

$$\hat{Y}_{(k')} \pm t_{n-m-1;\alpha/2} \cdot \hat{S}_{\text{Res}} \cdot \sqrt{1 + (1, \mathbf{x}_{(\mathbf{k}')})(\mathbf{X}'\mathbf{X})^{-1}(1, \mathbf{x}_{(\mathbf{k}')})'}. \qquad \text{(II.ii)}$$

Accordingly, the Bonferroni-adjusted limits for simultaneously predicting n' new observations (at possibly different levels) are

$$\hat{Y}_{(k')} \pm t_{n-m-1;\alpha/(2n')} \cdot \hat{S}_{\text{Res}} \cdot \sqrt{1 + (1, \mathbf{x}_{(\mathbf{k}')})(\mathbf{X}'\mathbf{X})^{-1}(1, \mathbf{x}_{(\mathbf{k}')})'}. \qquad \text{(II.ii, cont.)}$$

Prediction Interval for the Sample Mean of a New Sample of Controls

Now we use the parameter estimator from the original sample for predicting the $Y_{(1)}$ values of n_{c2} new control subjects by $\hat{Y}_{(1)} := (1, \mathbf{x}_{(\mathbf{1})})\cdot\hat{\beta} = \hat{\beta}_0$. We want to construct an interval around $\hat{\beta}_0$ in which the sample mean M_{c2} lies with probability $1 - \alpha$ if the LM (equation A2) is true: In analogy to the above difference variable U, we now determine the distribution of the difference variable

$V := M_{c2} - \hat{\beta}_0$ under equation A2. Because M_{c2} is normally distributed with expectation β_0 and variance $\frac{\sigma^2}{n_{c2}}$, it follows in analogy to above that the $(1 - \alpha)$ prediction limits for the sample mean in any new sample of n_{c2} controls are given by

$$\hat{\beta}_0 \pm t_{n-m-1;\alpha/2} \cdot \hat{S}_{\text{Res}} \cdot \sqrt{\frac{1}{n_{c2}} + (1, \mathbf{x}_{(\mathbf{1})})(\mathbf{X}'\mathbf{X})^{-\mathbf{1}}(1, \mathbf{x}_{(\mathbf{1})})'} \quad \text{(II.i)}$$

Acknowledgments

The authors thank D. Y. von Cramon for providing the opportunity to recruit and test patients in the Day Clinic for Cognitive Neurology, University of Leipzig, Germany; Sebastian Fischer for conducting part of the tests; and Dieter Heyer for helpful discussions on statistical details. Further, we are grateful to two anonymous reviewers for helping us to improve the article in several important issues. This work was supported by the Deutsche Forschungsgemeinschaft, grant PO 548/6-1 to S. P. and grant MU 2775/1-1 to G. M. P.

Reprint requests should be sent to Gisela Mueller-Plath, Department of Psychology, Martin-Luther-University Halle-Wittenberg, Brandbergweg 23, Halle, Germany 06108, or via e-mail: gisela.mueller-plath@psych.uni-halle.de.

Notes

1. Note that for binary variables, Pearson's $r^2 = \phi^2 = \chi^2 / n$.
2. Although in the original version of STRAVIS we explicitly assumed two distinct processing stages—computing a saliency map and deploying attention—this is not a critical assumption. We presently favor the notion that attention is deployed from the beginning and, while dwelling on a group of items, continuously modulates perception and thereby not only the target detection but also the saliency map. In STRAVIS, the attentional focus size is a stochastic variable with a variation the origin of which is not specified in detail.
3. Most likely, it also depends on the geometrical arrangement of the items, but this is neither being varied nor modeled in the present STRAVIS version.
4. The number of movements and the number of dwells are random variables the value of which depends mainly on the size of the attentional focus, the starting position of the search, and the target position. The expectations of the RTs are fitted to the empirical mean RTs in the different experimental conditions.
5. Note that the first is equivalent to a *t* test with $(n_0 + n_C - 1)$ degrees of freedom and the second to an *F* test with $(n_P - m - 1)$ and $(n_C - 1)$ degrees of freedom at significance level $\alpha = .10$, where $n_P = 28$ and $n_C = 28$ denote the number of patients and controls, n_0 the number of patients without any relevant lesion, and m the number of predictors in the model.
6. Note that this cannot be seen from the center of the confidence intervals as shown in Table 3 because the *F* distribution is asymmetrical about 1.

REFERENCES

Akaike, H. (1974). A new look at the statistical model identification. *IEEE Transactions on Automatic Control, 19,* 716–723.

Armstrong, K. M., & Moore, T. (2007). Rapid enhancement of visual cortical response discriminability by microstimulation of the frontal eye field. *Proceedings of the National Academy of Sciences, U.S.A., 104,* 9499–9504.

Braak, H., & Braak, E. (1991). Neuropathological staging of Alzheimer-related changes. *Acta Neuropathologica, 82,* 239–259.

Brefczynski, J. A., & DeYoe, E. A. (1999). A physiological correlate of the "spotlight" of visual attention. *Nature Neuroscience, 2,* 370–374.

Brickenkamp, R. (1962). *Test d2. Aufmerksamkeits-Belastungs-Test* [in German]. Göttingen: Hogrefe.

Carr, V. J., Dewis, S. A. M., & Lewin, T. J. (1998). Preattentive visual search and perceptual grouping in schizophrenia. *Psychiatry Research, 79,* 151–162.

Chelazzi, L. (1999). Serial attention mechanisms in visual search: A critical look at the evidence. *Psychological Research, 62,* 195–219.

Chen, Q., Marshall, J. C., Weidner, R., & Fink, G. R. (2009). Zooming in and zooming out of the attentional focus: An fMRI study. *Cerebral Cortex, 19,* 805–819.

Corbetta, M., Akbudak, E., Conturo, T. E., Snyder, A. Z., Ollinger, J. M., Drury, H. A., et al. (1998). A common network of functional areas for attention and eye movements. *Neuron, 21,* 761–773.

Corbetta, M., Miezin, F. M., Dobmeyer, S., Shulman, G. L., & Petersen, S. E. (1991). Selective and divided attention during visual discriminations of shape, color, and speed: Functional anatomy by positron emission tomography. *Journal of Neuroscience, 11,* 2383–2402.

Corbetta, M., Patel, G., & Shulman, G. L. (2008). The reorienting system of the human brain: From environment to theory of mind. *Neuron, 58,* 306–324.

Corbetta, M., & Shulman, G. L. (2002). Control of goal-directed and stimulus-driven attention in the brain. *Nature Reviews Neuroscience, 3,* 201–215.

Crick, F. (1984). Function of the thalamic reticular complex: The searchlight hypothesis. *Proceedings of the National Academy of Sciences, U.S.A., 81,* 4586–4590.

Davenport, N. D., Sponheim, S. R., & Stanwyck, J. J. (2006). Neural anomalies during visual search in schizophrenia patients and unaffected siblings of schizophrenia patients. *Schizophrenia Research, 82,* 15–26.

Donner, T. H., Kettermann, A., Diesch, E., Ostendorf, F., Villringer, A., & Brandt, S. A. (2002). Visual feature and conjunction searches of equal difficulty engage only partially overlapping frontoparietal networks. *Neuroimage, 15,* 16–25.

Duncan, J., & Humphreys, G. W. (1989). Visual search and stimulus similarity. *Psychological Review, 96,* 433–458.

Duncan, J., & Humphreys, G. W. (1992). Beyond the search surface: Visual search and attentional engagement. *Journal of Experimental Psychology: Human Perception and Performance, 18,* 578–588.

Eglin, M., Robertson, L. C., & Knight, R. T. (1991). Cortical substrates supporting visual search in humans. *Cerebral Cortex, 1,* 262–272.

Fels, M., & Geissner, E. (1996). *Neglect-Test (NET)*. Göttingen: Hogrefe.

Fimm, B., Zahn, R., Mull, M., Kemeny, S., Buchwald, F., Block, F., et al. (2001). Asymmetries of visual attention after circumscribed subcortical vascular lesions. *Journal of Neurology, Neurosurgery and Psychiatry, 71,* 652–657.

Findlay, J. M., & Walker, R. (1999). A model of saccade generation based on parallel processing and competitive inhibition. *Behavioral and Brain Sciences, 22,* 661–674.

Foster, J. K. (2001). Selective attention in Alzheimer's disease. *Frontiers in Bioscience, 6,* 135–153.

Fox, F. (1997). *Applied regression analysis, linear models, and related methods*. Thousand Oaks: Sage.
Friedrich, F. J., Egly, R., Rafal, R. D., & Beck, D. (1998). Spatial attention deficits in humans: A comparison of superior parietal and temporal-parietal junction lesions. *Neuropsychology, 12,* 193–207.
Gitelman, D. R., Nobre, A. C., Parrish, T. B., LaBar, K. S., Kim, Y. H., Meyer, J. R., et al. (1999). A large-scale distributed network for covert spatial attention: Further anatomical delineation based on stringent behavioural and cognitive controls. *Brain, 122,* 1093–1106.
Greenaway, R., & Plaisted, K. C. (2005). Top–down attentional modulation is stimulus specific. *Psychological Science, 16,* 987–994.
Greenlee, M. W., Berg, H., Stuhr, V., & Mergner, T. (2000). Visual search and visual working memory in patients with chronic focal cortical lesions. *Vision Research, 40,* 3759–3773.
Greenwood, P. M., Parasuraman, R., & Alexander, G. E. (1997). Controlling the focus of spatial attention during visual search: Effects of advanced aging and Alzheimer disease. *Neuropsychology, 11,* 3–12.
Greenwood, P. M., Sunderland, T., Friz, J. L., & Parasuraman, R. (2000). Genetics and visual attention: Selective deficits in healthy adult carriers of the epsilon 4 allele of the apolipoprotein E gene. *Proceedings of the National Academy of Sciences, U.S.A., 97,* 11661–11666.
Gronwall, D. M. (1977). Paced auditory serial-addition task: A measure of recovery from concussion. *Perceptual and Motor Skills, 44,* 367–373.
Hays, W. L. (1994). *Statistics* (5th ed.). Fort Worth: Harcourt Brace College Publishers.
Heße, U., Wienrich, C., Melzer, A., & Müller-Plath, G. (submitted). Eye movements and attention in visual feature search with graded target-distractor-similarity.
Hocking, R. T. (1996). *Methods and applications of linear models: Regression and the analysis of variance*. New York: Wiley.
Hodsoll, J., Mevorach, C., & Humphreys, G. W. (2009). Driven to less distraction: rTMS of the right parietal cortex reduces attentional capture in visual search. *Cerebral Cortex, 19,* 106–114.
Horowitz, T. S., Choi, W. Y., Horvitz, J. C., Cote, L. C., & Mangels, J. A. (2006). Visual search deficits in Parkinson's disease are attenuated by bottom–up target salience and top–down information. *Neuropsychologia, 44,* 1962–1977.
Humphreys, G. W., & Riddoch, M. J. (2001). Detection by action: Neuropsychological evidence for action-defined templates in search. *Nature Neuroscience, 4,* 84–88.
Husain, M., Mannan, S., Hodgson, T., Wojciulik, E., Driver, J., & Kennard, C. (2001). Impaired spatial working memory across saccades contributes to abnormal search in parietal neglect. *Brain, 124,* 941–952.
Juan, C. H., Muggleton, N. G., Tzeng, O. J., Hung, D. L., Cowey, A., & Walsh, V. (2008). Segregation of visual selection and saccades in human frontal eye fields. *Cerebral Cortex, 18,* 2410–2415.
Kastner, S., DeWeerd, P., Desimone, R., & Ungerleider, L. C. (1998). Mechanisms of directed attention in the human extrastriate cortex as revealed by functional MRI. *Science, 282,* 108–111.
Kim, J. N., & Shadlen, M. N. (1999). Neural correlates of a decision in the dorsolateral prefrontal cortex of the macaque. *Nature Neuroscience, 2,* 176–185.
Lamb, M. R., Robertson, L. C., & Knight, R. T. (1990). Component mechanisms underlying the processing of hierarchically organized patterns: Inferences from patients with unilateral cortical lesions. *Journal of Experimental Psychology: Learning, Memory & Cognition, 16,* 471–483.
Lewis, J. W., & Van Essen, D. C. (2000). Mapping of architectonic subdivisions in the macaque monkey, with emphasis on parieto-occipital cortex. *Journal of Comparative Neurology, 428,* 79–111.
Mallows, C. L. (1973). Some comments on Cp. *Technometrics, 15,* 661–675.
Mannan, S. K., Mort, D. J., Hodgson, T. L., Driver, J., Kennard, C., & Husain, M. (2005). Revisiting previously searched locations in visual neglect: Role of right parietal and frontal lesions in misjudging old locations as new. *Journal of Cognitive Neuroscience, 17,* 340–354.
Monosov, I. E., Trageser, J. C., & Thompson, K. G. (2008). Measurements of simultaneously recorded spiking activity and local field potentials suggest that spatial selection emerges in the frontal eye field. *Neuron, 57,* 614–625.
Moore, T., & Armstrong, K. M. (2003). Selective gating of visual signals by microstimulation of frontal cortex. *Nature, 421,* 370–373.
Moore, T., & Fallah, M. (2004). Microstimulation of the frontal eye field and its effects on covert spatial attention. *Proceedings of the National Academy of Sciences, U.S.A., 95,* 8981–8984.
Müller, N. G., Bartelt, O. A., Donner, T. H., Villringer, A., & Brandt, S. A. (2003). A physiological correlate of the "Zoom Lens" of visual attention. *Journal of Neuroscience, 23,* 3561–3565.
Müller-Plath, G. (2000). *Formale Modellierung visueller Suchstrategien* [in German]. Leipzig: MPI Series.
Müller-Plath, G. (2008). Localizing subprocesses of visual search by correlating local brain activation in fMRI with response time model parameters. *Journal of Neuroscience Methods, 171,* 316–330.
Müller-Plath, G., Heße, U., Melzer, A., & Wienrich, C. (in preparation). StraViS 2.0: A revised model for visual feature search with graded target-distractor-similarity.
Müller-Plath, G., & Pollmann, S. (2003). Determining subprocesses of visual feature search with reaction time models. *Psychological Research, 67,* 80–105.
Nobre, A. C., Coull, J. T., Walsh, V., & Frith, C. D. (2003). Brain activations during visual search: Contributions of search efficiency versus feature binding. *Neuroimage, 18,* 91–103.
O'Shea, J., Muggleton, N. G., Cowey, A., & Walsh, V. (2004). Timing of target discrimination in human frontal eye fields. *Journal of Cognitive Neuroscience, 16,* 1060–1067.
Paus, T. (1996). Location and function of the human frontal eye field—A selective review. *Neuropsychologia, 34,* 475–483.
Pollmann, S., Mahn, K., Reimann, B., Weidner, R., Tittgemeyer, M., Preul, C., et al. (2007). Selective visual dimension weighting deficit after left lateral frontopolar lesions. *Journal of Cognitive Neuroscience, 19,* 365–375.
Pollmann, S., & von Cramon, D. Y. (2000). Object working memory and visuospatial processing: Functional neuroanatomy analyzed by event-related fMRI. *Experimental Brain Research, 133,* 12–22.
Pollmann, S., Weidner, R., Humphreys, G. W., Olivers, C. N. L., Müller, K., Lohmann, G., et al. (2003). Separating distractor rejection and target detection in posterior parietal cortex: An event-related fMRI study of visual marking. *Neuroimage, 18,* 310–323.
Ptak, R., & Valenza, N. (2005). The inferior temporal lobe mediates distracter-resistant visual search of patients with spatial neglect. *Journal of Cognitive Neuroscience, 17,* 788–799.
R Development Core Team. (2008). *R: A language and environment for statistical computing*. Vienna, Austria: R Foundation for Statistical Computing. Retrieved from http://www.R-project.org. Accessed Oct–Dec 2008.

Reitan, R. M. (1958). Validity of the trailmaking test as an indication of organic brain damage. *Perceptual and Motor Skills, 8,* 271–276.
Robinson, D. L., & Petersen, S. E. (1992). The pulvinar and visual salience. *Trends in Neuroscience, 15,* 127–132.
Schindler, I., Clavagnier, S., Karnath, H.-O., Derex, L., & Perenin, M.-T. (2006). A common basis for visual and tactile exploration deficits in spatial neglect? *Neuropsychologia, 44,* 1444–1451.
Shadlen, M. N., & Newsome, W. T. (1996). Motion perception: Seeing and deciding. *Proceedings of the National Academy of Sciences, U.S.A., 93,* 628–633.
Shallice, T. (1988). *From neuropsychology to mental structure*. Cambridge: University Press.
Soto, D., Humphreys, G. W., & Rotshtein, P. (2007). Dissociating the neural mechanisms of memory-based guidance of visual selection. *Proceedings of the National Academy of Sciences, U.S.A., 104,* 17186–17191.
Sprenger, A., Kömpf, D., & Heide, W. (2002). Visual search in patients with left visual hemineglect. *Progress in Brain Research, 140,* 395–416.
Thompson, K. G., & Bichot, N. P. (2005). A visual salience map in the primate frontal eye field. *Progress in Brain Research, 147,* 251–262.
Treisman, A., & Gormican, S. (1988). Feature analysis in early vision: Evidence from search asymmetries. *Psychological Review, 95,* 15–48.
Treisman, A. M., & Gelade, G. (1980). A feature-integration theory of attention. *Cognitive Psychology, 12,* 97–136.
Wickens, T. D. (1995). *The geometry of multivariate statistics*. Hillsdale: Erlbaum.
Wise, S. P., Boussaoud, D., Johnson, P. B., & Caminiti, R. (1997). Premotor and parietal cortex: Corticocortical connectivity and combinatorial computations. *Annual Reviews in Neuroscience, 20,* 25–42.
Wolfe, J. M. (1994). Guided search 2.0: A revised model of visual search. *Psychonomic Bulletin & Review, 1,* 202–238.
Wolfe, J. M. (1998). Visual search: A review. In H. Pashler (Ed.), *Attention* (pp. 13–73). London: University College London Press.
Zimmermann, P., & Fimm, B. (1994). *Testbatterie zur Aufmerksamkeitspruefung (TAP)* [in German]. Wuerselen: Psytest.